INVESTIGATION ON THE EFFECTS OF GRAPHENE IN P3HT AS AN ACTIVE LAYER IN SOLAR CELLS

FADILAH BINTI ABD WAHAB

FACULTY OF SCIENCE
UNIVERSITY OF MALAYA
KUALA LUMPUR

2019

INVESTIGATION ON THE EFFECTS OF GRAPHENE IN P3HT AS AN ACTIVE LAYER IN SOLAR CELLS

FADILAH BINTI ABD WAHAB

**DISSERTATION SUBMITTED IN FULFILMENT OF
THE REQUIREMENTS FOR THE DEGREE OF
MASTER OF SCIENCE**

**DEPARTMENT OF PHYSICS
FACULTY OF SCIENCE
UNIVERSITY OF MALAYA
KUALA LUMPUR**

2019

UNIVERSITY OF MALAYA
ORIGINAL LITERARY WORK DECLARATION

Name of Candidate: **FADILAH BINTI ABD WAHAB**

Matric No: **SGR 100053**

Name of Degree: **MASTER OF SCIENCE**

Title of Project Paper/Research Report/Dissertation/Thesis (“this Work”):

INVESTIGATION ON THE EFFECTS OF GRAPHENE IN P3HT AS AN ACTIVE LAYER IN SOLAR CELLS

Field of Study: **ORGANIC SOLAR CELLS**

I do solemnly and sincerely declare that:

(1) I am the sole author/writer of this Work;
(2) This Work is original;
(3) Any use of any work in which copyright exists was done by way of fair dealing and for permitted purposes and any excerpt or extract from, or reference to or reproduction of any copyright work has been disclosed expressly and sufficiently and the title of the Work and its authorship have been acknowledged in this Work;
(4) I do not have any actual knowledge nor do I ought reasonably to know that the making of this work constitutes an infringement of any copyright work;
(5) I hereby assign all and every rights in the copyright to this Work to the University of Malaya (“UM”), who henceforth shall be owner of the copyright in this Work and that any reproduction or use in any form or by any means whatsoever is prohibited without the written consent of UM having been first had and obtained;
(6) I am fully aware that if in the course of making this Work I have infringed any copyright whether intentionally or otherwise, I may be subject to legal action or any other action as may be determined by UM.

Candidate’s Signature Date:

Subscribed and solemnly declared before,

Witness’s Signature Date:

Name:

Designation:

INVESTIGATION ON THE EFFECTS OF GRAPHENE IN P3HT AS AN ACTIVE LAYER IN SOLAR CELLS

ABSTRACT

Presently, fullerenes have been the acceptor materials of the most intensively studied bulk heterojunction (BHJ) structure of Polymer Solar Cell (PSC). However fullerene and its derivatives have several disadvantages including high cost, poor morphological stability and limited absorption of light. The main aim of this study is to investigate the effects of graphene as an acceptor in PSC. Graphene is synthesized in this study using two methods; the first is the exfoliation process of graphite flakes into graphene sheets (GS) and secondly is the oxidation process of graphite flakes using Hummer's Method to form graphene oxide (GO). The experimental results of the synthesized GS are presented on the optical, structural, and morphological properties. Spin-coating method is utilized to form the blend thin films either on the glass or indium tin oxide (ITO) electrode. Doping of 2.5% GS obtained from exfoliation process into Poly(3-hexylthiophene) (P3HT), induces energy transfer at the P3HT:GS interface as indicated by the photoluminescence (PL) quenching in the blend film. Then, the blend film of P3HT:GS is deposited onto ITO electrode which covered with a thin layer of semi-transparent conducting polymer/poly(ethylene dioxythiophene):polystyrenesulfonic acid (PEDOT:PSS), to form ITO/PEDOT:PSS/P3HT:GS/Aluminium(Al) PSC device. In this study, the PSC efficiency has increased from 6.32 x 10-4% to 1.01 x 10-3%, for device without and with GS, respectively. In the second method of synthesis of this study, GO is successfully produced from Hummer's Method, as evident from the optical, structural, and morphological characterizations. Nevertheless the films consist of P3HT blended with GO do not show a PL quenching, indicating of no energy transfer at the P3HT:GO interface. This PL result shows that the synthesized GO produced from Hummer's method is non-effective acceptor material to be used as an active layer in PSC application.

Keywords: Graphene sheets, graphene oxide, poly(3-hexylthiophene), active layer, polymer solar cell

PENYIASATAN KE ATAS KESAN GRAFINA DALAM P3HT SEBAGAI LAPISAN AKTIF DALAM SEL SURIA

ABSTRAK

Pada masa ini, fullerina adalah bahan penerima struktur simpang-hetero pukal (BHJ) yang paling kerap dikaji bagi Sel Suria Polimer (PSC). Walau bagaimanapun, fullerina dan derivatifnya mempunyai beberapa kelemahan termasuklah kos yang tinggi, kestabilan morfologi yang lemah dan penyerapan cahaya yang terhad. Tujuan utama kajian ini adalah untuk mengkaji kesan-kesan grafina sebagai penerima dalam PSC. Grafina disintesis dalam kajian ini menggunakan dua kaedah; yang pertama ialah proses pengelupasan kepingan grafit kepada lembaran grafina dan yang kedua ialah proses pengoksidaan menggunakan Kaedah Hummer untuk menghasilkan grafina oksida (GO). Hasil eksperimen grafit yang disintesis ditunjukkan melalui sifat optik, struktur dan morfologi. Kaedah salutan-putaran telah digunakan bagi menghasilkan campuran filem nipis sama ada di atas kaca ataupun pada elektrod indium timah oksida (ITO). Penambahan sebanyak 2.5% GS yang diperoleh daripada proses pengelupasan ke dalam Poli (3-hexylthiophene) (P3HT) mendorong pemindahan tenaga antara muka pada P3HT:GS seperti yang ditunjukkan oleh sepuh lindap fotoluminasi dalam filem campuran. Kemudian, campuran filem P3HT:GS diletakkan di atas elektrod indium timah oksida yang diliputi dengan lapisan nipis separa-lutsinar konduksi polimer/ poli (ethylene dioxythiophene):asid polistrenesulfonic (PEDOT: PSS), untuk membentuk peranti PSC, ITO/PEDOT:PSS/P3HT:GS/ Aluminium. Dalam kajian ini, kecekapan PSC telah meningkat daripada 6.32 x 10-4% kepada 1.01 x 10-3%, untuk peranti masing-masing tanpa GS dan dengan GS. Bagi kaedah sintesis yang kedua kajian ini, grafina oksida (GO) berjaya dihasilkan daripada Kaedah Hummer, seperti yang dibuktikan melalui ciri-ciri optik, struktur dan morfologi. Walau bagaimanapun, filem-filem yang terdiri daripada P3HT yang dicampur dengan GO tidak menunjukkan sepuh lindap PL, menunjukkan tiada pemindahan tenaga pada antara muka P3HT:GO. Hasil PL ini menunjukkan bahawa sintesis GO yang dihasilkan dari Kaedah Hummer adalah bahan yang tidak berkesan untuk digunakan sebagai penerima di lapisan aktif dalam aplikasi PSC.

Kata kunci: Lembaran grafina, grafina oksida, poli(3-hexylthiophene), lapisan aktif, sel suria polimer

ACKNOWLEDGEMENTS

Alhamdulillah. Thanks to Allah S.W.T.

First and foremost, let me thank my supervisor Assoc. Prof. Dr. Khaulah Sulaiman for her advising and guidance of this thesis. She has been the biggest influence on my education and development as a researcher. She has helped steer me straight each of the many times I have run into difficulties that were beyond my control.

Many thanks as well to my co-supervisor, Dr. Huang Nay Ming for his continuing guidance and support. He gave me a lot of brilliant ideas throughout the experiments and delivered valuable comments to improve the quality of this thesis.

I would never have gotten to this point without the love and support from my family, especially my late father, Abd Wahab Salimin, my mother, Sopiah Zainol and my beloved siblings, Noor Ashida, Roziana, Siti Rohana, Siti Ainei, Siti Norli, Mohd Aminuddin and Mohd Fadil. I love you all and will never be able to repay for all the supportive and encouraging words that you have given me.

I owe a very special thanks to all Low Dimensional Materials Research Centre (LDMRC) members for their sincere guidance on the experiments and analysis of the results. They have been more generous than I would have ever hoped for. I also would like to thank my group members, Toong Way Yun, Zurianti, Lim Lih Wei, Muhammad Saipul and Shahino Mah for their help during experiments and conferences.

Finally, A big thanks to the Physics Department of University of Malaya. I am indebted to all of the department members for what they have taught me during my time here. It has been a pleasure to be a part of this department. Thanks to all the lecturers and members of department for helping me get through all these past years.

TABLE OF CONTENTS

LIST OF FIGURES

LIST OF TABLES

LIST OF SYMBOLS AND ABBREVIATIONS

A : Absorbance

α : Absorption coefficient

I_{max} : Current at maximum power

θ : Diffraction angle

E_g : Energy gap

FF : Fill factor

t : Film thickness

P_{in} : Input power

d : Interatomic spacing distance

P_{max} : Maximum power

R_a : Mean surface roughness

V_{oc} : Open circuit voltage

P_{out} : Output power

η : Power conversion efficiency

I_{sc} : Short-circuit current

J_{sc} : Short-circuit current density

T : Transmittance

V_{max} : Voltage at maximum power

λ : Wavelength

AM 1.5 : Air mass 1.5

BHJ : Bulk heterojunction

CB : Conduction band

HOMO : Highest occupied molecular orbital

ITO	:	Indium tin oxide
LUMO	:	Lowest unoccupied molecular orbital
P3HT	:	Poly(3-hexylthiophene)
PCBM	:	[6,6]-phenyl-C_{61}-butyric acid methyl ester
PCE	:	Power conversion efficiency
PEDOT:PSS	:	Poly(3,4-ethylenedioxythiophene) poly(styrenesulfonate)
PSCs	:	Polymer solar cells
PT	:	Poly(thiophene)
PV	:	Photovoltaic
RMS	:	Root-mean-square
rpm	:	Rotations per minute
SMU	:	Source measuring unit
STC	:	Standard test condition
VB	:	Valence band

CHAPTER 1: INTRODUCTION

1.1 Motivation and Research Overview

These days, the increase in population and advances in technology root the growth of energy consumption. As we know, world-wide energy consumption rapidly increasing year by year. Nowadays, most of the energy dependence on fossil fuels is gradually being replaced by alternative energies. Renewable energy is important because it has a clean source of energy that has much lower environmental impact and will not run out compared to the conventional energy.

Solar energy is one of the main sources of natural energy and will never be coming to an end unless the sun explodes. Although the sun has a powerful source of energy, humans are faced with the challenge of capturing sunlight that can be used as a source of energy. Thus, the research in photovoltaic (PV) cells will be very important to supply the demand in the future. Development in solar energy research can give a significant impact in improving energy capacity and also meet the requirements of users in a variety of lifestyle in the future.

Closest example we can see is the statistics of energy consumption in our country, Malaysia. As seen in the Figure 1.1 (Malaysian Energy Commission, 2015) energy consumption is very high in the industrial and transport sectors and rising year by year since 1978. Only in 2007, the industrial sector is showing the energy consumption is significantly reduced but still high compared to the other sectors. This trend is seen as unhealthy for the long term if the energy supplied is insufficient to accommodate the addition of this energy consumption. Figure 1.2 shows the primary energy supply in Malaysia from 1978 until 2013 (Malaysian Energy Commission, 2015).

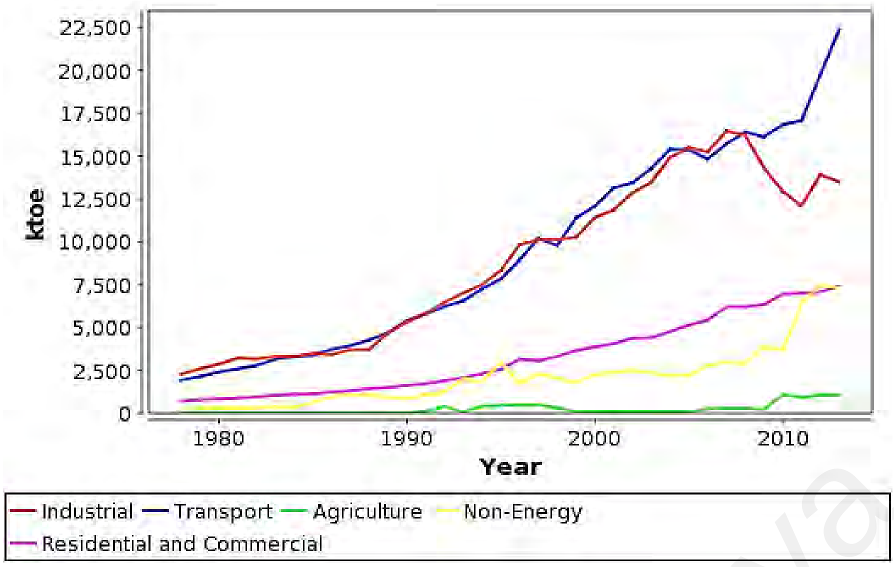

Figure 1.1: The statistics of final energy demand in Malaysia (Malaysian Energy Commission, 2015).

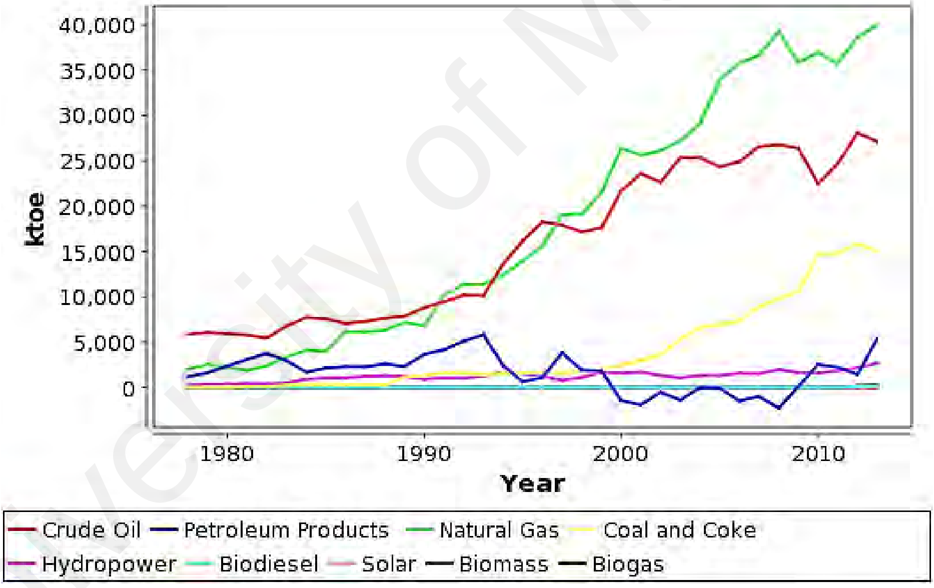

Figure 1.2: The statistics of primary energy supply in Malaysia (Malaysian Energy Commission, 2015).

Based on the data statistics from Malaysian Energy Commission, something has to be done to increase the power capacity for accommodating the energy demand. Renewable energy such as solar energy is one of way that can be explored to increase the capacity of energy. For that, a device to convert sunlight into energy is required. A device that converts the radiation of the sun to electricity is called PV cell or solar cell. The idea of PV cell started from leaves, which are every leaf of green plant convert sunlight to chemical energy. Pigments such as chlorophyll were used to sensitize titanium-based materials (O'Regan & Grätzel, 1991; Tang & Albrecht, 1975).

The most common materials used in solar energy to convert sunlight into electrical energy or so-called PV effects are inorganic materials (Goetzberger et al., 2003; Miles et al., 2007). However, other than inorganic materials, various efforts also have been made to develop PV cells using organic materials within the last three decades (Brabec et al., 2002; Günes et al., 2007; Thompson et al., 2005; Wöhrle & Meissner, 1991).

Organic PV devices have low production costs and environment-friendly manufacturing methods on large area, light and flexible substrates, which increase the attention among the researchers in the last few years (Christoph et al., 2001; friend, 2004). Since the first reports more than 30 years ago on molecular thin film devices, their power conversion efficiencies have increased significantly from 0.001% (Tang & Albrecht, 1975) to 1% (Tang, 1986) and in year 2005 up to 5.5% (Rand et al., 2005; Reyes-Reyes et al., 2005; Xue et al,, 2005). Increases in the efficiency of energy produced by organic photovoltaic devices continue to attract the attention of researchers working to produce higher energy efficiency.

In this research, graphene will be used as an acceptor in the active layer of PSC aim to increase the efficiency of these PV devices. Graphene is the only two dimensional crystal of sp^2 hybridized carbon. Graphene was experimentally demonstrated to be stable at ambient conditions which has gained much attention among researchers. At room temperature, this gapless semiconductor with unique electronic properties reaches its electron mobility 10 000 $cm^2 V^{-1} s^{-1}$ (Morozov et al., 2008).

This dissertation focuses on experimenting the methods available to synthesized graphene and observes the effects of the graphene as an acceptor in polymeric based PV cells. Graphene materials used in this study will be self-synthesized using two main methods. After graphene has been synthesized, the material will be characterized and later used in the PV active layer to fabricate PV devices. A research study in PSC using a p-type conjugated polymer with graphene incorporating in the active layer is presented.

1.2 History of Polymer Solar Cell (PSC)

The PV effect was first revealed by French physicist A. E. Becquerel in 1839, which discovered a photocurrent when platinum electrodes, covered with silver bromide or silver chloride, was illuminated in aqueous solution (Becquerel, 1839). After over 30 years, the reports on photoconductivity have been made as a result of research on selenium (Adams & Day, 1877). In the early twentieth century, photoconductivity was observed for the first organic compound, which was called Anthracene (Pochettino, 1906; Volmer, 1913). Then in 1958, Kearns and Calvin worked with magnesium phthalocyanines (MgPh) and successfully measured a photovoltage of 200 mV (Kearns & Calvin, 1958).

In the early 1960, many common dyes such as methylene blue have been discovered to have semiconductor properties (Bube, 1960). These organic materials later were observed to have photovoltaic effect along with biological molecules such as carotenes, chlorophylls and other porphyrins, also the structural related phthalocyanines (PC) marked as one of the important discoveries in PV cell research. In general, discovery and research of solar cells have begun almost 200 years ago and constantly making a lot of new discoveries to bring this research to a higher level. Table 1.1 shows some important milestone in the field of research since it was first explored (Spanggaard & Krebs, 2004).

Table 1.1: Some important milestone in the development of PSC.

Year	Development in Polymer Solar Cell
1839	Becquerel observed the photoelectrochemical process.
1906	Pochettino studied the photoconductivity of anthracene.
1958	Kearns and Calvin worked with magnesium phthalocyanines (MgPh), measuring a photovoltage of 200 mV.
1964	Delacote observed a rectifying effect when magnesium phthalocyanines (MgPh) was placed between two different metal electrodes.
1986	Tang published the first heterojunction PV device.
1991	Hiramoto made the first dye/dye bulk heterojunction PV by co-sublimation.
1993	Sariciftci made the first polymer/C_{60} heterojunction device.
1994	Yu made the first bulk polymer/C_{60} heterojunction PV.
1995	Yu / Hall made the first bulk polymer/polymer heterojunction PV.
2000	Peters / van Hal used oligomer-C_{60} dyads/triads as the active material in PV cells.
2001	Schmidt-Mende made a self-organised liquid crystalline solar cell of hexabenzocoronene and perylene.
2001	Ramos used double-cable polymers in PV cells.

Research in this twenty first century revealed for obtaining high efficiency various factors need to be in serious note such as solvent selection where the high efficiency could be obtained up to 2.5% (Shaheen et al., 2001). Besides that, morphology optimization also plays an important role to increase PSCs efficiencies and have provided power conversion efficiencies (PCEs) of 4–5% that draw global interests in PSCs (Chen et al., 2009; Ma et al., 2005). The developing novel acceptors can also improve the efficiency and for example is paper reported by Zhao managed to get a high efficiency PV cell of 6.5% using C_{60} with an indene bisadduct (Zhao et al., 2010).

In recent years, there are numerous high-performance polymers have been developed. For example, one of the impressive polymers is composed of thieno[3,4-b]-thiophene (TT) and benzodithiophene (BDT) alternating units (Carsten et al., 2011; Duan et al., 2016). This polymer donor system managed to achieve PCEs of 7–8%. Following this work, PCEs of more than 7% were frequently reported with either new materials or novel device optimization techniques (Li et al., 2012; Liang et al., 2010; Liu et al., 2014; Zhou et al., 2011).

1.3 History of Graphene as a Recent Star in Materials Science.

In the 1930's, Landau and Peierls claimed that strictly two-dimensional (2D) crystals were thermodynamically unstable and because of that those materials theoretically could not exist (Landau, 1937; Peierls, 1935). The reason for this is the theory pointed out that a divergent contribution of thermal fluctuations in low-dimensional crystal lattices would lead to such displacements of atoms and for that they become comparable to interatomic distances at any finite temperature (Landau & Lifshitz, 1980). Mermin later described crystalline order in two dimensions and strongly supported by a whole compilation of experimental observations (Mermin, 1968).

For a long time 2D materials were presumed not to be existent without a 3D base. A major breakthrough happened in 2004, when Novoselov experimentally discovered graphene (Novoselov et al., 2004) and other free-standing 2D atomic crystals as for example, single-layer boron nitride and half-layer BSCCO (Novoselov et al., 2005). This significant discovery observed these crystals could be obtained on top of non-crystalline substrates (Novoselov et al., 2005; Zhang et al., 2005), in liquid suspension (Novoselov et al., 2004; Stankovich et al., 2006) and as suspended membranes (Meyer et al., 2007).

1.4 Research Objectives

The main objective of this research is to investigate the effects of graphene on the performance of solar cells. The second objective is to synthesize graphene using two main methods and characterize their optical, structural, and morphology properties. The third objective is to prepare graphene/Poly(3-hexylthiophene)P3HT blend thin films and also characterize the optical properties and morphology.

The objectives of this research are summarized below.

i. To investigate the effects of graphene as an acceptor in PSC.

ii. To synthesize and characterize the optical properties and morphology of graphene/GO.

iii. To prepare graphene/Poly(3-hexylthiophene), P3HT thin films and characterize the optical properties and morphology.

1.5 Thesis Outline

Chapter 1 states about the necessity of energy in our daily lives as renewable energy is one of the important sources of energy. This section tells about the significance of research in solar energy and the development efforts need to be continued. History of the PSC and graphene as a recent rising star in materials science are also discussed as a knowledge base for this research. Then, the objectives of this research work are included in this section as well.

Chapter 2 of this dissertation explains the literature review and the theory related to this research. The subtopics included are organic materials which explain the properties of conjugated polymer as a donor and graphene material as an acceptor in active layer of polymer solar cells. Then, basic working principles and types of device architectures of PSC will also be explained in this chapter.

In Chapter 3, the experimental methodology involved in this research work is discussed. For this chapter the subtopic included is methods to synthesize graphene using two approaches which are oxidation process and exfoliation process. Later on following with solutions preparation, thin films preparation, device fabrication and also Aluminium (Al) electrode deposition via thermal evaporation method. Additionally, characterization aspects will also be explained in this chapter.

Chapter 4 will be focusing on the two main methods to synthesize graphene. The first one will be via exfoliation process using sonication method and the second method will be via oxidation process using Hummer's method. The results obtained are shown focusing on the optical, structural, morphology of the synthesized graphene. Several trial methods are used to get a homogenous blend film of P3HT:GO. Then, P3HT:GO blend films are characterized by PL spectroscopy to check the presence of PL quenching as an indication of an energy transfer from P3HT to GO. This stage of characterization is the critical point to determine the outcome of the efficiency of solar cells. The effects of GO as active layer in PSC are discussed.

In Chapter 5, GS synthesized via exfoliation process using sonication method are used to fabricate PSC. Then, further discussion on the electrical properties of GS as an acceptor in the active layer of PSC are presented. Analysis and discussion on the effects of GS as an acceptor in PSC are reported based on the results of experiments.

Finally, Chapter 6 is the conclusion from the studies that have been conducted. In addition, some future works are also proposed in this chapter so that the results of this study will be developed further in the future. Figure 1.3 shows the summaries of the research methodology that has been carried out in this work.

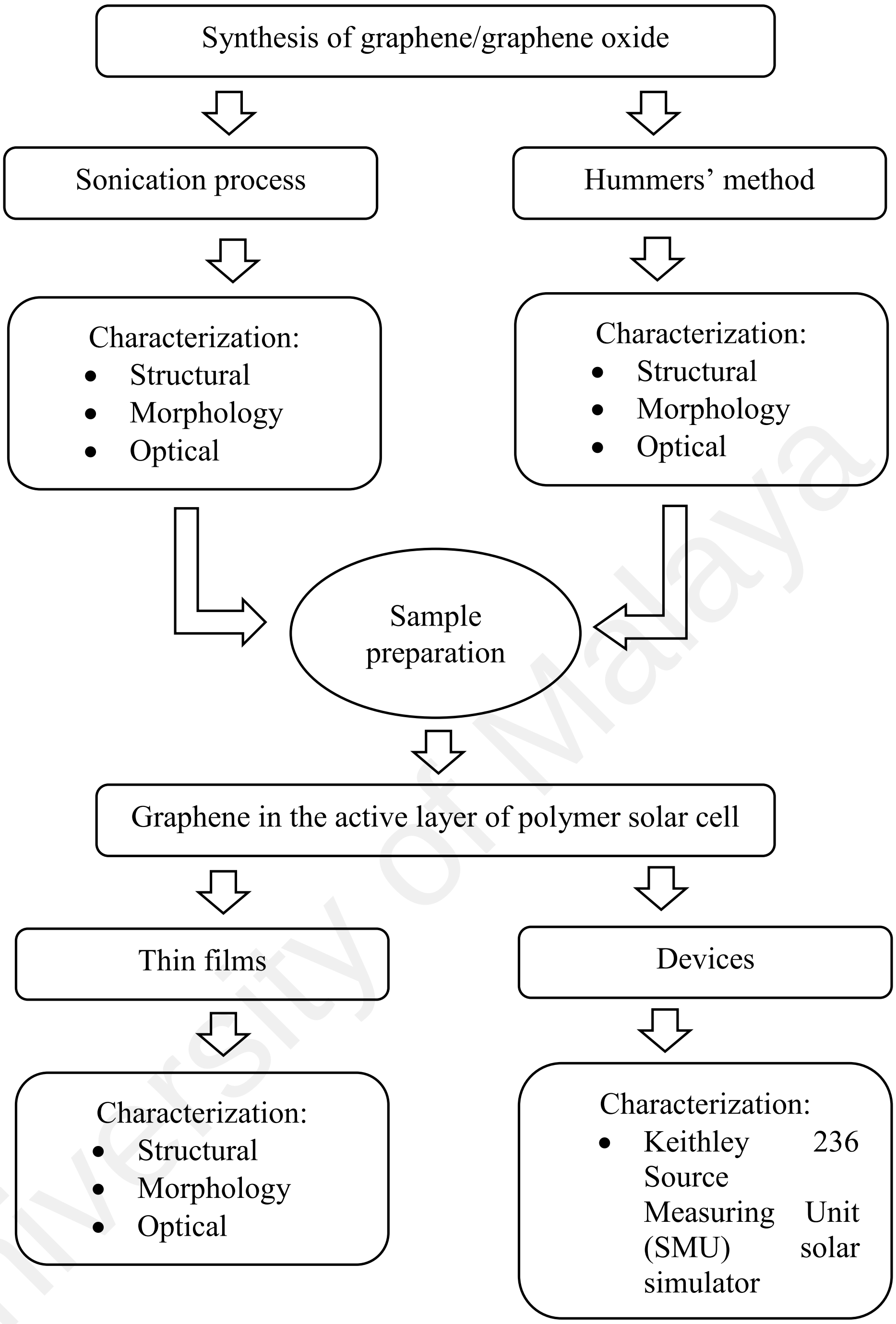

Figure 1.3: Block diagram of research methodology in this study.

CHAPTER 2: THEORY AND LITERATURE REVIEW

2.1 Overview

In this chapter, the theories related to the research that will be carried out are discussed. At first, this chapter will explain the basic operation and several types of device architecture of PSC. After that, the discussion will be about conjugated polymers. Lastly, the discussion will be about donor and acceptor materials used to make PSC. P3HT and graphene will be deliberated in more details for a better understanding of their respective functions.

2.2 Polymer Solar Cell

Polymer Solar Cell (PSC) represents as one of exciting class in renewable energy technology because they are lightweight, flexible and have a low production cost. For these reasons there are growing amount of research enthusiastic in PSC to potentially searching for less expensive types of solar cells such as those based on organic dyes and polymers. The efficiency of these devices has enhanced significantly for the last two decades through the development in PSC such as solution-processed bulk heterojunction (BHJ). Nowadays, fullerenes have been the most studied acceptor materials in BHJ PSC. However research is currently on the move to investigate non-fullerene molecular acceptors that can improve the efficiency of the device better.

Figure 2.1 shows the latest research cell efficiency provided by National Renewable Energy Laboratory (NREL), United States Department of Energy. The highest efficiency for organic cells in various types is recorded by SCUT-CSUfor 15.6%. While for organic tandem cells the record is hold by SCUT/eFlexPV with the efficiency recorded up to 13.2%.

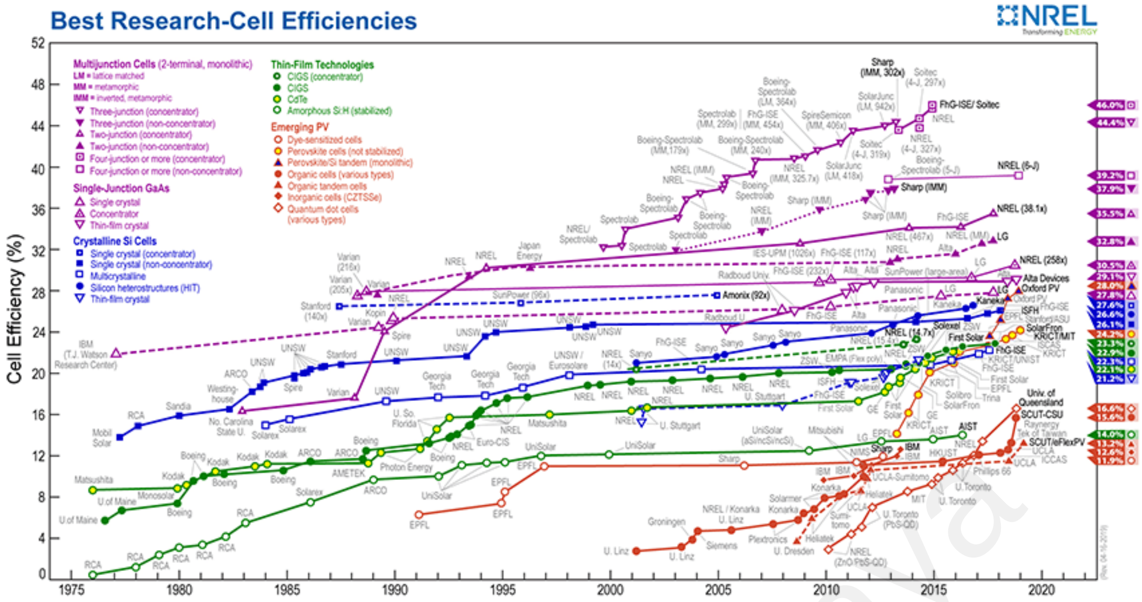

Figure 2.1: The latest efficiency provided by NREL, U.S. (NREL & National Renewable Energy Laboratory, 2019)

2.2.1 Basic Working Principles of Polymer Solar Cell

PSC which converts light into electricity commonly has a planar-layered structure, where the organic light-absorbing layer is sandwiched between two different electrodes. One of the electrodes must be semi-transparent such as Indium–tin-oxide (ITO), however a thin metal layer can be used as well. The other electrode, which is frequently used is aluminium but calcium, magnesium, gold and others are also can be used. Fundamentally, the basic principle of a light-harvesting PSC is the reverse of the principle in light emitting diodes (LED) as shown in Figure 2.2 (Spanggaard & Krebs, 2004).

A LED emits light when initiated. This happens when an electron is introduced at the low-work function electrode (cathode) and a hole at the high-work function electrode (anode). Then, at certain point the electron and the hole encounter, and upon recombination light is emitted (Burroughes et al., 1990; Friend et al., 1997; Greenham et al., 1993).

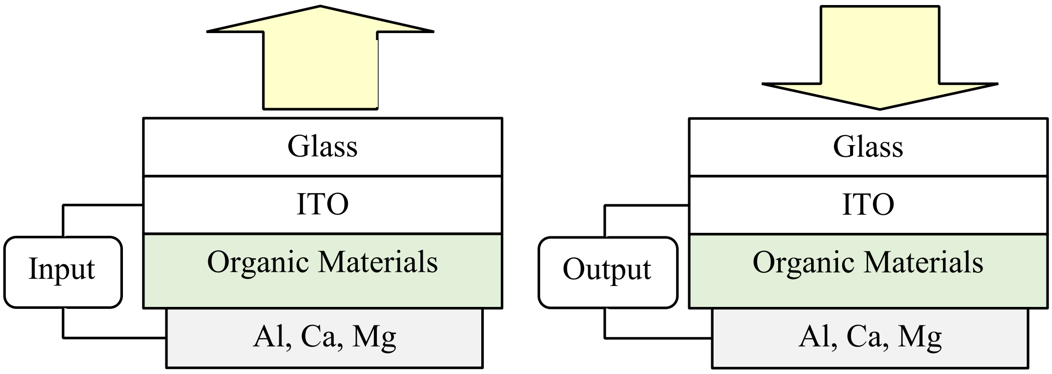

Figure 2.2: A PSC device on the right is the reverse of a LED device on the left. Adapted from (Spanggaard & Krebs, 2004).

The principle of PSC is contrary to the LED. Once light is absorbed, an exciton formed when an electron is promoted from the highest occupied molecular orbital (HOMO) to the lowest unoccupied molecular orbital (LUMO). This process must be followed by exciton dissociation where the electron must then reach one electrode while the hole must reach the other electrode. The asymmetrical ionization energy/work functions of the electrodes provide electrical field in order to achieve charge separation. The process of light harvesting including the placing of energy levels is illustrated in Figure 2.3 (Spanggaard & Krebs, 2004).

In PSC, when an excited electron is generated by incident light it will recombine with its hole rapidly. Therefore, something must be done to separate them before recombination can take place. According to this behaviour, PSC requires two materials to prevent the occurrence of recombination which one that electrons prefer and the other that holes prefer.

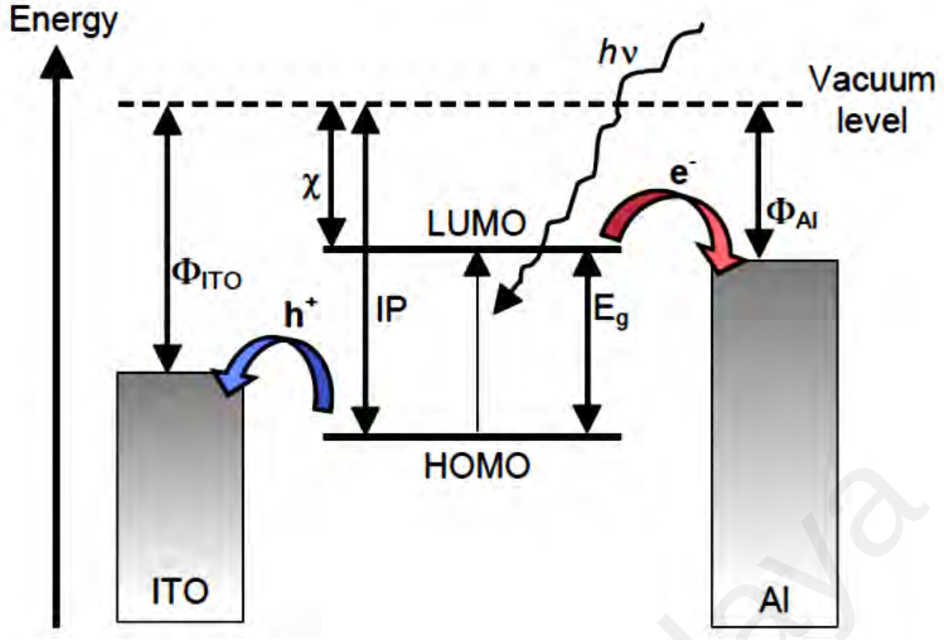

Figure 2.3: Energy levels and light harvesting (Spanggaard & Krebs, 2004).

In recent years, numerous architectures for PSC have been investigated in order to improve the efficiencies. In general, for a successful organic photovoltaic cell three important processes have to be optimized to obtain a high conversion efficiency of solar energy into electrical energy. Reducing energy and voltage loss is a vital area of improvement for the design of PSCs. Significant amounts of energy are lost in the context of charge generation and charge recombination compared with their inorganic counterparts (Matthew et al., 2018).

For PSC operation principle, the process of the photon-to-electron conversion can be divided into four basic steps (Li et al., 2018) which are photon absorption (η_A), exciton diffusion (η_{ED}), charge carrier transfer (η_{CT}), and charge carrier collection (η_{CC}). These four aspects are very important elements to consider with the aim to get higher efficiencies in PSC. The aspect of each step is elaborated further in order to understand more regarding the process of the photon-to-electron conversion.

2.2.1.1 Absorption of Light

The materials those making up the active layer are responsible for the absorption of light in the PSC. These materials are characterized by having a certain gap energy (E_g) which indicates the energetic separation between the valence electrons and the nearest free electronic states. In Figure 2.3, the difference between the HOMO and LUMO is defined as:

$$E_g = E_{LUMO} - E_{HOMO} \tag{2.1}$$

When E_g is larger than the thermal energy available at room temperature, material is commonly considered as semiconductor. Valence electrons cannot be excited to the conduction states simply by thermal activation. The absorption of a photon of energy greater than E_g can excite an electron from the HOMO to the LUMO state:

$$E_{photon} = \frac{c.h}{\lambda photon} \geq E_g \tag{2.2}$$

where λ_{photon} is the wavelength of the light, c is the speed of light and h is Planck's constant. As shown in Figure 2.3, a vacant valence state, termed a 'hole' leaves behind after the absorption of the photon by excitation and the photon energy now be existing as the potential energy difference between this excited electron-hole pair. Nevertheless, as there is a continuous sequence of states above the LUMO level, the excited electron will rapidly undergo thermal relaxation, ending up at the LUMO level. All of the photon energy exceeding the gap energy will be lost as heat is defined as:

$$E_{thermal\ loss} = E_{photon} - E_g \tag{2.3}$$

2.2.1.2 Exciton diffusion

The morphology plays important part on exciton diffusion (η_{ED}).The generated excitons in photon absorption process transport through diffusion. In order to convert to charge carrier, this exciton should move to the donor–acceptor interface within its lifetime. (Li et al., 2018).

2.2.1.3 Charge Transport

In PSC, the electron-hole pair is held together by coulomb forces, creating a quasi-particle called an exciton but to generate electricity the electron and hole must be parted, and then collected at electrodes of opposite polarity. Therefore, the exciton bond must be broken to accomplish this. For this reason, an organic semiconductor is introduced in the active layer, which has an energetically lower lying LUMO-level. The material with the highest LUMO is called the electron donor whereas the other is called the electron acceptor. In order for electron transfer to be favourable the following condition must be true, with E_{exc-b} is the exciton bond energy:

$$E_{donorLUMO} - E_{acceptorLUMO} \geq E_{exc-b} \tag{2.4}$$

In PSC, the donor material is frequently a conjugated polymer, while the acceptor is often a small molecule based on the C60 fullerene. The absorption of the highly symmetric C60 molecule is relatively low compared with the highly absorbing donor polymer. Most of the excitons are produced in the donor phase and electrons are shifted to the acceptor. For excitons generated in the acceptor, the following must hold right in order for holes to be shifted from the acceptor to the donor:

$$E_{donorHOMO} - E_{acceptorHOMO} \geq E_{exc-b} \tag{2.5}$$

The specific distance between an exciton generation site and a donor/acceptor interface must be on order of 5-10 nm as the exciton only has a certain lifetime before the electron recombines with the hole (Deibel & Dyakonov, 2010). At the same time, the photons need to cross a certain thickness of active layer around 100 nm, in order for most of them to be absorbed. Because of that, the donor-acceptor structure in the active layer is the main key for the efficiency of the PSC.

2.2.1.4 Charge Collection

The electron and hole will transport to the acceptor and donor phases respectively once the separation of the exciton into an electron and a hole at a donor/acceptor interface occurres. To produce current the charges must be collected at separate electrodes as shown in Figure 2.4 in which the holes need to be collected at the anode and electrons at the cathode. The current flow is controlled by the use of electrodes having different work functions. Hence, the anode electrode is selected as a high work function material and the cathode chosen as a low work function metal. In this case, the holes will transport to the high work function anode and the electrons to the low work function cathode as shown in Figure 2.4.

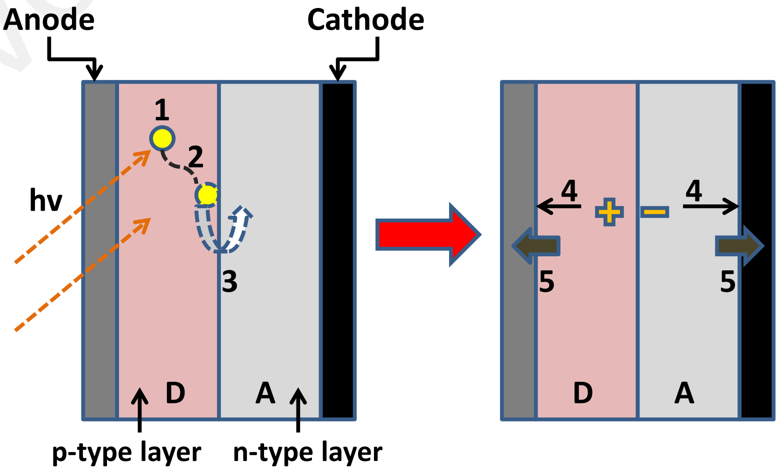

Figure 2.4: The schematic drawing of the working principle of PSC.

2.2.2 Characterization Parameters of the Polymer Solar Cell

Solar cells are characterized by measuring the current-voltage curve under illumination of a light source. The metal-insulator-metal (MIM) (Sze & Ng, 2007) model is suitable to describe this characteristic as organic semiconductors show very low intrinsic carrier concentration. Figure 2.5 (i) illustrates the current delivered by a solar cell under zero bias is called short circuit current (I_{SC}). This happens because exciton dissociation and charge transport is driven by the so-called built-in potential. This potential is identical to the difference in work function (W_f) of the hole and electron collecting electrodes. For PSC, the transparent ITO electrode is frequently chosen ($W_{f,ITO}$ = 4.7 eV) in combination with a low work function material ($W_{f,Ca}$ = 2.87 eV, $W_{f,Mg}$ = 3.66 eV, $W_{f,Al}$ = 4.24 eV) (Michaelson, 1977) as counter-electrode to achieve a high internal field (Bharathan & Yang, 1998; Kim et al., 1998; Park et al., 1996).

In (ii) the voltage where the current equals zero is called open circuit voltage (Voc). This situation is defined by the case where the band is flat, since the applied voltage equals the difference in the work function of the electrodes. When $V > Voc$, (Figure 2.5 (iii)), the diode is biased in the forward direction. Electrons are now injected from the low work function electrode into the LUMO and holes from the high work function electrode into the HOMO of the organic layer, respectively.

In (iv) When $V < 0$, the diode is driven under a reverse biased condition the solar cells works as a photodiode. The field is higher than in (i) which often leads to enhanced charge generation and collection efficiency.

Maximum power point is the point where the electrical power $P = I \times V$ reaches the maximum value signifies the situation where the solar cell can supply its maximum power to an external load. The ratio of this maximum electrical power, P_{max} to the product of the short circuit current and the open circuit voltage is called the fill factor (FF):

$$FF = \frac{Pmax}{Isc \times Voc} \tag{2.6}$$

Preferably, the fill factor should be unity but losses due to transport and recombination result in values between 0.2 – 0.7 for organic photovoltaic devices. The photovoltaic power conversion efficiency (η) is then calculated for an incident light power P_{light}:

$$\eta = \frac{I_{sc} \times V_{oc} \times FF}{P_{light}} \tag{2.7}$$

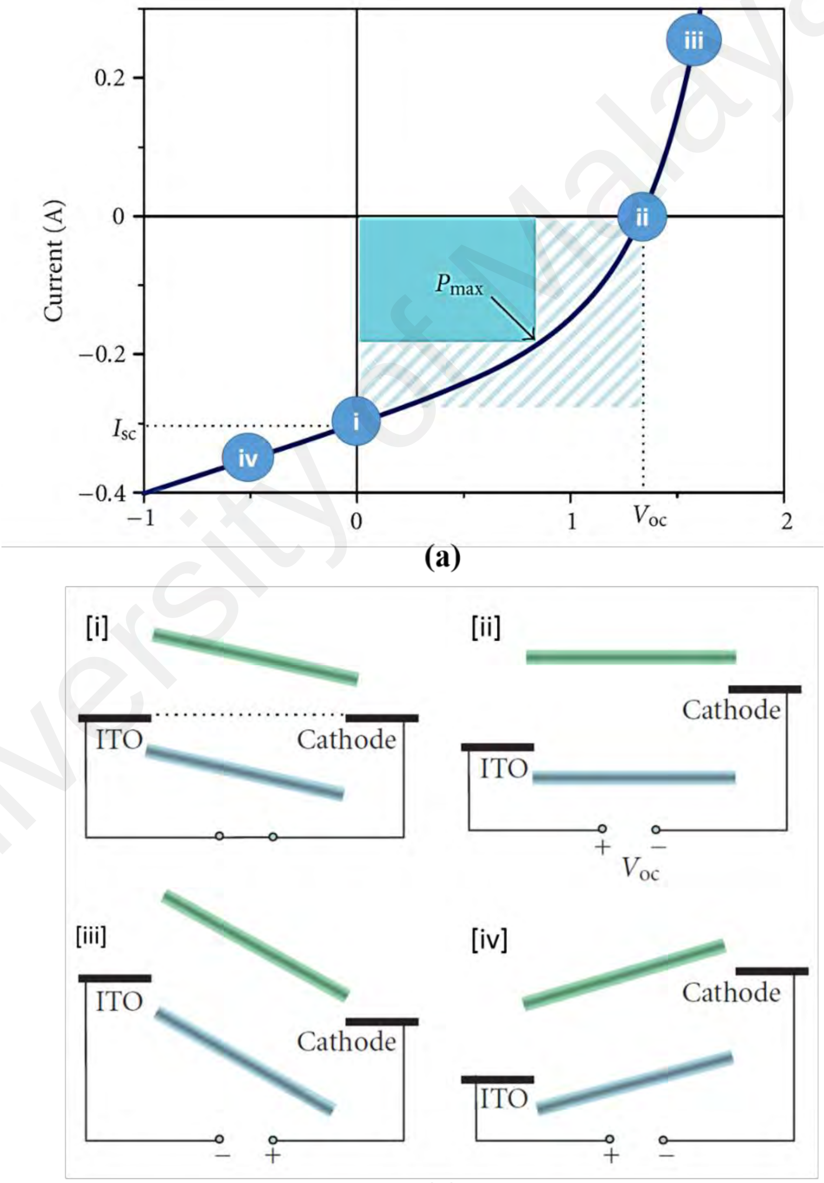

(a)

(b)

Figure 2.5: Current (voltage) characteristics of a typical organic diode shown together with the metal-insulator-metal picture for the characteristic points (a) Short circuit condition, (b) Open circuit condition, (c) Forward bias and (d) Reverse bias (Kietzke, 2007).

The key parameters for a solar cell which are *Jsc*, *Voc, η* and *FF* have to be determined under particular illumination condition which is the standard test condition (STC). A schematic diagram of the current density-voltage curve to characterize PSC under illumination is shown in Figure 2.6.

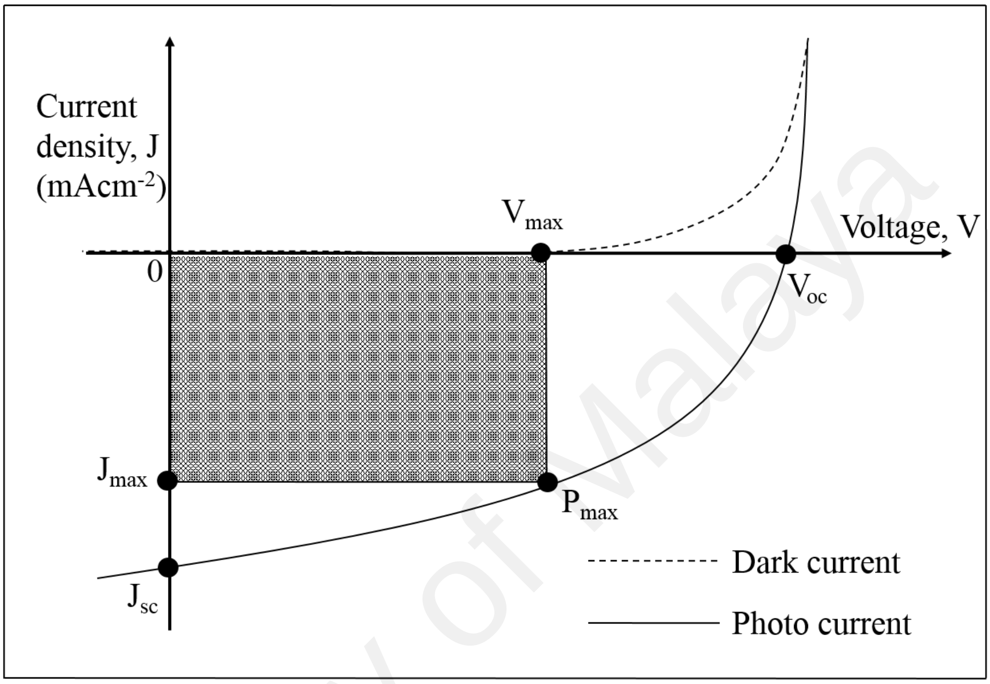

Figure 2.6: Ideal current density-voltage characteristics of a polymer solar cell.

2.2.3 Device Architectures for Polymer Solar Cell

There are several types of junctions for PSC such as single layer, bilayer and bulk heteronjunction (BHJ) have been established in this solar cell research. These device architectures will be discussed regarding their individual advantages and disadvantages. For these device architectures, the difference lies in the exciton dissociation process in the photoactive layer. Further issue that plays an important role is the consecutive charge transport to the electrodes in PSC.

2.2.3.1 Single Layer Homojunction

Single layer homojunction is the first type of PSC device architecture. Single layer homojunction is a type of PSC that contains a layer of organic electronic material between two conductive electrodes. A layer of indium tin oxide (ITO) with high work function and a layer of low work function metal such as Aluminum, Calcium or Magnesium are the typical conductors that can be used to fabricate PSC. The single layer homojunction structure of PSC is shown in Figure 2.7. The structure of single layer homojunction is very basic and simple to fabricate but this device architecture does not work so well. This happens because the electrons frequently recombine with the holes without reaching the electrode.

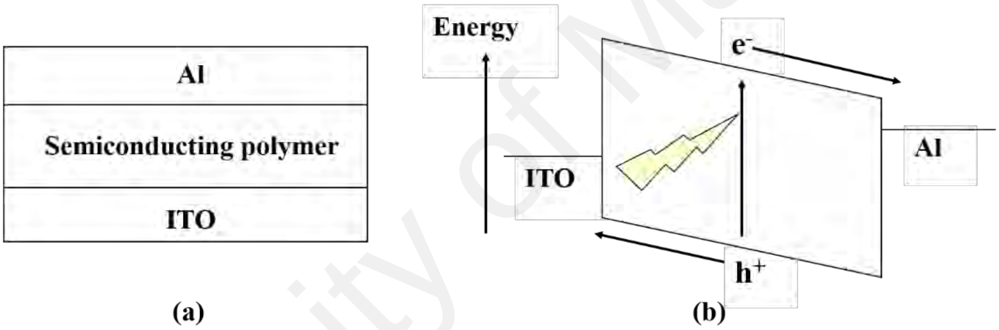

Figure 2.7: (a) The basic structure of a single layer solar cell and (b) Working principle.

2.2.3.2 Bilayer Heterojunction

Bilayer heterojunction is a type of PSC that contains two layers of materials between two metallic conductors. The active layer of an ideal BHJ solar cell is defined as a bicontinuous interpenetrating network of donor and acceptor at the nanometer scale with maximum interfacial area. Excitons can always reach the donor-acceptor interface within their limited diffusion length and charge separation can occur efficiently (Ramírez et al., 2015). For efficient charge carriers, the bilayer materials have to be corresponding according to the donor HOMO and the acceptor LUMO. Bilayer heterojunction device structure splits excitons much more efficiently compared to the single layer PSC. Even though bilayer heterojunction is much better compared to single layer homojunction structure, the thickness of polymer layer needs to be very thin to make it work efficiently. Typically the thickness of PSC is around 100 nm and merely a small fraction of the excitons can reach the heterojunction interface in this type of PSC architecture. The bilayer heterojunction of polymer solar cell is shown in Figure 2.8.

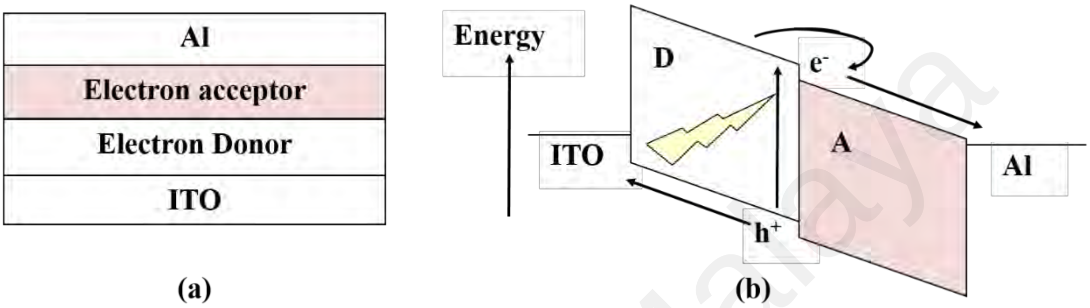

Figure 2.8: (a) The basic structure of a bilayer solar cell and (b) Working principle.

2.2.3.3 Bulk Heterojunction (BHJ)

Bulk heterojunction device structure consists a layer consisting of a blend of donor and acceptor materials. Bulk heterojunction structure is a better structure of PSC compared to single layer homojunction and bilayer heterojunction. This is because the active layer can made thick enough for effective photon absorption without the difficulties of exciton dissociation compared to bilayer heterojunction PSC structure. The Figure 2.9 shows the structure of a bulk heterojunction in PSC.

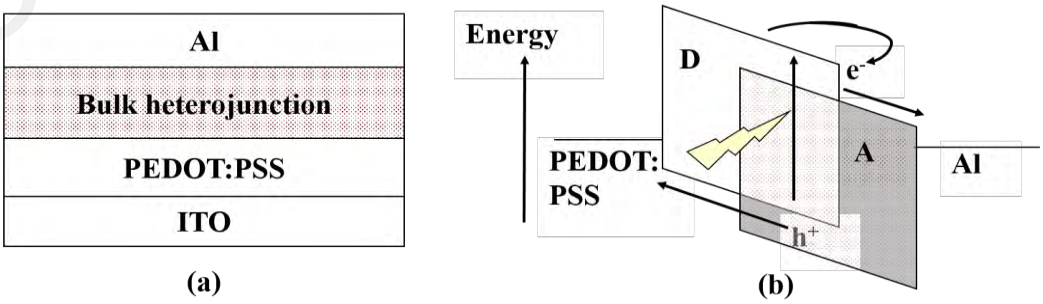

Figure 2.9 : (a) The basic structure of a bulk heterojunction solar cell and (b) Working principle.

2.3 Conjugated Conducting Polymers

In 2000, the Nobel Committee awarded Heeger, MacDiarmid and Shirakawa the Nobel Prize for Chemistry which acknowledged their ground-breaking contribution for discovery of conductive polymer (Heeger, 2001; MacDiarmid, 2001; Shirakawa, 2001). Originally the modern study of electric conduction in conjugated polymers began in 1977 describing the doping of polyacetylene with the publication by the group at the University of Pennsylvania (Chiang et al., 1977). Unusual optoelectronic properties let conjugated polymers to be used for a huge number of applications, such as protecting metals from corrosion, sensing devices, artificial actuators, all-plastic transistors, non-linear optical devices and light emitting displays. These new technologies are thought to compliment current inorganic-based optoelectronic devices, which greatly impacted our society starting from the second half of the 20th century.

2.3.1 Charge Transport Characteristics

Conducting polymers are both electronically conducting polymers and ionically conducting polymers. In order for polymers to be electronically conductive they must possess not only charge carriers but also an orbital system that allows the charge carriers to move. The repeat units and conductivities for some common conjugated polymers can be seen in Table 2.1 (Dai, 1999).

2.3.2 Electronic Properties

According to band theory (Harrison, 1979), the electrical properties of direct gap inorganic semiconductors are determined by their electronic structures, and the electrons move within discrete energy states called bands. The energy difference between them is called the band gap. Electrons must have certain energy to occupy a given band and need extra energy to move from the valence band to the conduction band. Moreover, the bands should be partially filled in order to be electrically conducting, as neither empty nor full bands can carry electricity.

Table 2.1: Some conjugated conducting polymers.

Polymer (date conductivity discovered)	Structure	d-d* gap (eV)	Conductivity[#] (S/cm)
I. Polyacetylene and analogues			
Polyacetylene (1977)	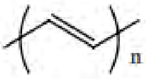	1.5	$10^3 – 1.7\times10^5$
Polypyrrole (1979)	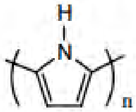	3.1	$10^2 – 7.5\times10^3$
Polythiophene (1981)		2.0	$10 – 10^3$
II. Polyphenylene and analogues			
Poly(paraphenylene) (1979)	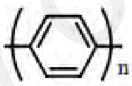	3.0	$10^2 – 10^3$
Poly(p-phenylene vinylene) (1979)	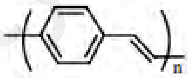	2.5	$3 – 5\times10^3$
Polyaniline (1980)		3.2	30 – 200

Based on Figure 2.10(a), metals have high conductivities. The energy bands of insulators and semiconductors, however, are either completely full or completely empty. For instance, most conventional polymers have full valence bands and empty conduction bands, which are separated from each other by a wide energy gap as in Figure 2.10(b). In contrast, conjugated polymers have narrower band gaps as can be seen in Figure 2.10(c) and doping can change their band structures by either taking electrons from the valence band (*p*-doping) or adding electrons to the conduction band (*n*-doping).

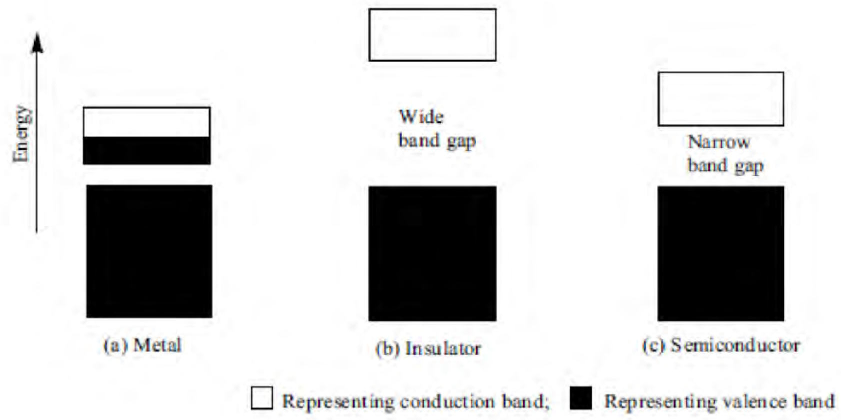

Figure 2.10: A schematic representation of energy gaps in (a) metal, (b) insulator and (c) semiconductor (Dai, 1999).

2.4 Donor Materials

The donor material contributes electrons and primarily transports holes. The donor plays a significant role as the absorber to photon which means donor materials necessity is a wide absorption range to match the solar spectrum. Besides, another requirement for good donor is a great hole or electron mobility to maximize charge transport, which also can be applied to acceptor.

Polythiophenes (PTs) are one of the significant classes of conjugated polymers with a wide series of application in various fields. PTs are really important such as in field-effect transistors, conducting films and so on. As shown in Figure 2.11, PTs are formed from the polymerized thiophenes with sulfur heterocycle and become conducting via doping process. This happens when electrons are added or removed from the conjugated π-orbitals.

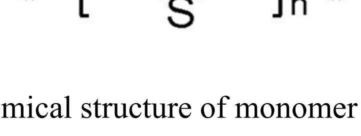

Figure 2.11: The chemical structure of monomer repeating unit of PTs.

In comparison with polypyrrole and polyaniline, polythiophene (PT) possesses a narrower bandgap and a higher oxidation doping potential, which indicates that polythiophene can be both p-doped by oxidation and n-doped by reduction. The higher oxidation doping potential results in lower stability of the p-doped conducting polythiophene in comparison with conducting polypyrrole and polyaniline (Li & Qian, 1993). However, it makes the neutral polythiophene stable, which guarantees the optoelectronic applications of polythiophene as semiconducting polymers.

2.5 Acceptor Material

Numerous organic compounds exhibit potential properties as electron acceptor material and up to now fullerene and its derivatives are the most effective electron acceptor materials. However due to the high price of fullerene and its derivatives, researchers are now looking for a new substitute cost-effective material. Therefore, in this experiment graphene is chosen to be used as the acceptor material in the bulk heterojunction (BHJ) PSC.

2.5.1 Carbon

Carbon was discovered as charcoal in prehistoric times. The name of the carbon discoverer is never known and was first not recognised as an element until much later. Carbon is the chemical element with symbol C and atomic number 6. It is nonmetallic and tetravalent as a member of group 14 on the periodic table. Carbon is making four electrons available to form covalent chemical bonds. Some allotropes of carbon are shown in Figure 2.12.

2.5.2 Graphene

Graphene is a flat monolayer of carbon atoms tightly packed into a two-dimensional (2D) honeycomb lattice and is a basic building block for graphitic materials of all other dimensionalities. It can be wrapped up into 0D fullerenes, rolled into 1D nanotubes or stacked into 3D graphite as shown in Figure 2.13. Graphene (or "2D graphite") has attracted many researchers and been studied for more than sixty years (McClure, 1956; Slonczewski & Weiss, 1958; Wallace, 1947).

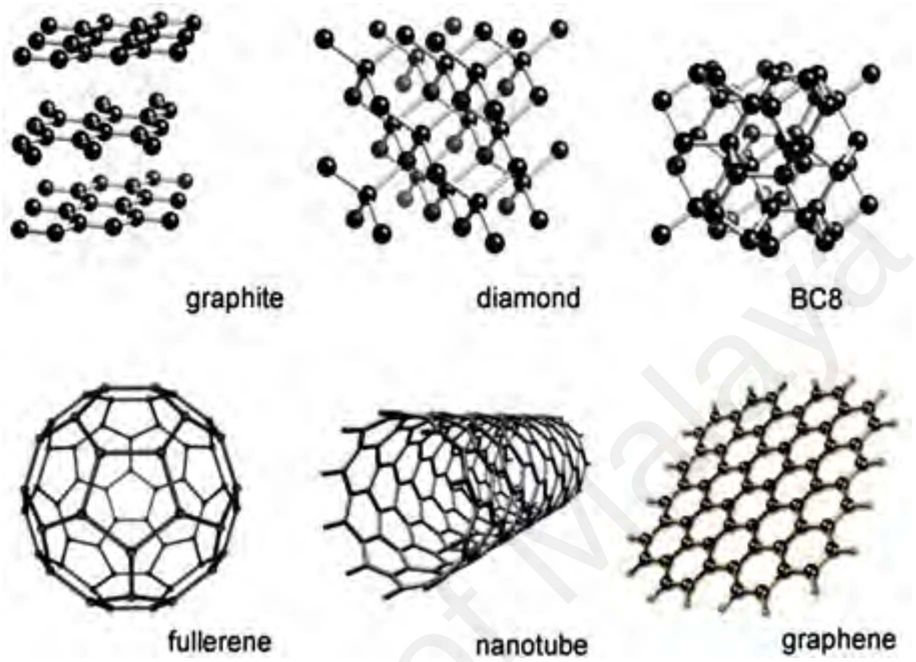

Figure 2.12: Some allotropes of carbon (Oganov et al., 2013).

2.5.3 Graphene from Graphite Oxide

Graphite oxide has been mainly produced by the Brodie (Brodie, 1859), Staudenmaier (Staudenmaier, 1898) and Hummers (Hummers & Offeman, 1958) methods. All three methods involve oxidation of graphite in the presence of strong acids and oxidants. The level of the oxidation can be varied on the basis of the method, the reaction conditions and the precursor graphite used. Although extensive research has been done to reveal the chemical structure of graphite oxide, several models are still being debated in the literature.

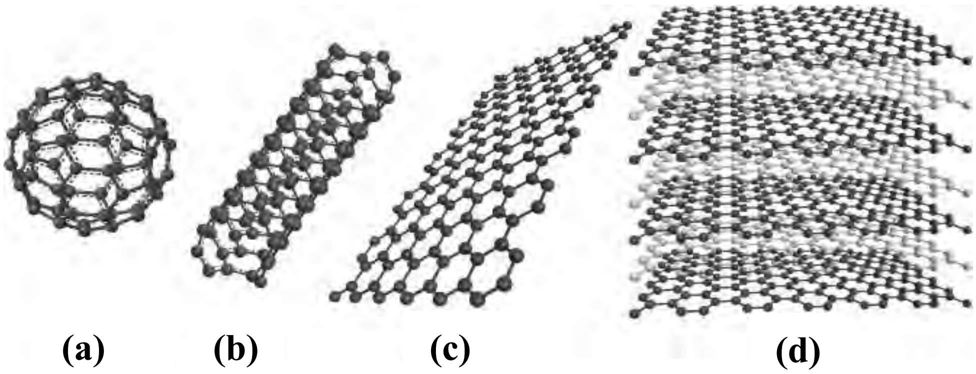

Figure 2.13: Forms of sp^2-bonded carbon (a) Fullerene, (b) Single-walled carbon nanotubes, (c) Graphene and (d) Graphite (Pumera et al., 2010).

The sp^2-bonded carbon network of graphite is strongly disrupted and a significant fraction of this carbon network is bonded to hydroxyl groups or participates in epoxide groups (Cai et al., 2008; He et al., 1998; He et al., 1996; Lerf et al., 1998). Minor components of carboxylic or carbonyl groups are thought to populate the edges of the layers in graphite oxide. This indicates that further work with solid-state NMR on 13C-labelled graphite oxide is necessary, along with titration as an example with fluorescent tags of carboxylic and other groups to identify their spatial distribution on individual GO platelets derived from graphite oxide as discussed further below.

Graphite oxide consists of layered structure of 'graphene oxide' sheets that are strongly hydrophilic such that intercalation of water molecules between the layers readily occurs (Buchsteiner et al., 2006; Lerf et al., 2006). The interlayer distance between the GO sheets increases reversibly from 6 to 12 Å with increasing relative humidity (Buchsteiner et al., 2006). Notably, graphite oxide can be completely exfoliated to produce aqueous colloidal suspensions of GO sheets by simple sonication (Stankovich et al., 2007) and by stirring the water/graphite oxide mixture for a long enough time (Jung et al., 2007). The measurement of the surface charge (zeta potential) of GO sheets (D. Li et al., 2008) shows that they have negative charges when dispersed in water. This suggests that electrostatic repulsion between negatively charged GO sheets could generate a stable aqueous suspension of them. A considerable body of work (Boehm et al., 1962; Scholz & Boehm, 1969) on such aqueous colloidal suspensions was carried out in the 1950s and 1960s. Such GO sheets probably have a similar chemical structure to the layers in graphite oxide and are a promising starting material in the generation of colloidal suspensions of other chemically modified graphene (CMG) through chemical tuning. Filtration of CMG suspensions has produced free-standing paper-like materials (Chen et al., 2008; Dikin et al., 2007; Li et al., 2008; Xu et al., 2008), that have a layered structure. Significant advances have also been made in using homogeneous suspensions of CMG sheets to produce thin films, which can be relevant to transparent and electrically conductive thin-film applications, among others (Eda et al., 2008; Si & Samulski, 2008; Xu et al., 2008)

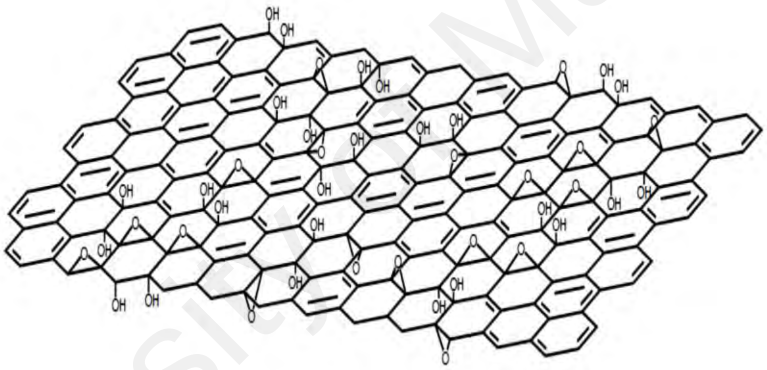

Figure 2.14: Chemical structure of graphite oxide (He et al., 1998).

2.5.4 Graphene Oxide Sheets

Several authors have stated that homogeneous colloidal suspensions of GO in aqueous and various organic solvents can be achieved by simple sonication of graphite oxide (Parades et al., 2008; Park et al., 2008; Stankovich et al., 2007; Stankovich et al., 2006). The hydrophilic GO can be easily dispersed in water at concentrations up to 3 mg ml^{-1} (Park et al., 2008; Stankovich et al., 2007; Stankovich et al., 2006) affording brown/dark-brown suspensions. The exfoliation to achieve GO sheets has been typically confirmed by thickness measurements of the single graphene sheet approximately ~1 nm height on substrates such as mica using atomic force microscopy (AFM).

Graphite oxide can be dispersed directly in several polar solvents such as ethylene glycol, DMF, NMP and THF at about 0.5 mg ml^{-1} (Parades et al., 2008). It has also been shown that the chemical modification of GO sheets by organic molecules yields homogeneous suspensions in organic solvents (Stankovich et al., 2006), reaction of graphite oxide with isocyanate groups produced isocyanate-modified GO sheets that are well dispersed in polar aprotic solvents. It was proposed that carbamate and amide functional groups are generated by the reaction of isocyanate with hydroxyl and carboxyl groups (Stankovich et al., 2006).

The amide-coupling reaction (Tasis et al., 2006) between the carboxyl acid groups of GO and octadecylamine (after $SOCl_2$ activation of the COOH groups) was used (Niyogi et al., 2006) to modify GO by long alkyl chains with 20 wt% yield. Interestingly, chemical modification of an alternative starting material, graphite fluoride, with alkyl lithium reagents produced alkyl-chain-modified graphene sheets that could be dispersed in organic solvents after sonication (Worsley et al., 2007).

2.5.5 Previous reports on graphene-based polymer solar cells

Summary of graphene as conducting electrode is given in Table 2.2. The presented results show that graphene and related materials offered high transparency and low sheet resistance along with high stability and strength. This evidences that the performance of the photovoltaic devices is continuously improving by incorporating graphene and its novel composites. Therefore, graphene and related materials are advantageous over conventional materials for anodic applications in photovoltaic technology (Iqbal & Rehman, 2018).

Table 2.2: Summary of previous work on graphene in solar cell applications.

Materials	**Structure of solar cell**	**PCE (%)**	**Year**
CVD-Gr (Eletskii et al., 2015)	Quartz/Gr/PEDOT:PSS/CuPc:C60/BCP/Ag	0.85	2015
CVD-Gr (Kim et al., 2014)	P(VDF-TrFE)/Gr/PEDOT/PSS/ P3HT/PCBM/Ca/Al	2.07	2014
CVD-Gr (Dong et al., 2014)	Glass/Pt grids/Gr/TiO2/dye/ Electrolyte/counter electrode	0.4	2014
rGO (Jeon et al., 2014)	Glass/ITO/HTL(rGO)/active layer/LiF/Al	3.71	2014
c-Si/GQDs (Gao et al., 2014)	In/Ga/c-Si/GQDs/Au	6.63	2014

In PSC, fill factor (*FF*) is equally important to PCE because its signifying the quality of the solar cell as a power source which defined as the ratio between the maximum power delivered to an external circuit. The enhancement of the conversion efficiency of the devices is due to the creation of continuous electrons pathways arising after an appropriate addition of graphene to P3HT. Table 2.3 shows photovoltaic parameters of the of polymer solar cells with different results of FF using graphene as acceptor material in recent studies (Bkakri et al., 2015). From the table, the highest FF is active layer with 1.5 wt% incorporated graphene.

Table 2.3: Photovoltaic parameters and PCE of the ITO/P3HT/Au and ITO/P3HT:Graphene/Au solar cells.

Graphene weight ratio (wt%)	V_{oc} **(V)**	J_{SC} **(A/cm^2)**	V_{max} **(V)**	J_{max} **(A/cm^2)**	***FF*** **(%)**
0	0.35	4.25×10^{-4}	0.19	2.34×10^{-4}	29
1.5	0.55	9.93×10^{-4}	0.35	6.4×10^{-4}	41
3	0.49	7.43×10^{-4}	0.30	4.73×10^{-4}	38
5	0.40	6.93×10^{-4}	0.24	4.03×10^{-4}	34

CHAPTER 3: EXPERIMENTAL METHODOLOGY

3.1 Chapter Overview

The details of the experimental methodology of this research work will be explained in this chapter. In this research, the self-synthesized materials used were GS and GO. For the first part, synthesis of GS and GO are discussed, followed by the preparation of the samples. Method for solar cell fabrication will be explained afterwards. In order to fabricate the active layer of PSC, the spin-coating technique was used in this study. The final part of this chapter will explain the characterization technique used in this research works such as UV-VIS/NIR spectrometer, surface profilometer, X-ray diffraction (XRD), micro Raman spectroscopy, atomic force microscopy (AFM), Fourier-transform infrared spectroscopy (FTIR) as well as field-emission scanning electron microscopy (FESEM). Solar cell electrical characterization method will also be discussed.

3.2 Synthesis of Graphene Sheets and Graphene Oxide

3.2.1 Chemicals and Materials

For this research of PSC, various types of materials were considered before fabricating a solar device such as organic materials, solvents, substrates and electrodes. In this research work, self-synthesized GO and GS were used instead of as-purchased. There were two methods used to synthesize graphene in this study, which will be compared later. The first method was exfoliation of graphite using sonication process and the second method was the synthesis of GO using Hummer's method. Comparing these two synthesis methods, the best result will be adapted for solar cell device.

3.2.2 Synthesis of Graphene Sheets Using Exfoliation Sonification Method

In this study, GS were produced via exfoliation process of graphite. 200 mg of graphite flake (3061, Asbury Graphite Mill Inc.) was placed in a vial. Then, 10 ml chloroform was added and the solution was sonicated for 6 hours. In order to get the thin sheets of graphene, the solution was later centrifuged at 4000 rpm for 20 minutes. The supernatant of the solution was then separated from the precipitate to obtain the GS as shown in Figure 3.1(a), Figure 3.1(b) and Figure 3.2.

Figure 3.1: (a) Graphite & GS in chloroform solution (b) Precipitate of graphite at the bottom.

Figure 3.2: GS in chloroform solution.

3.2.3 Synthesis of Graphene Oxide using Hummer’s Method

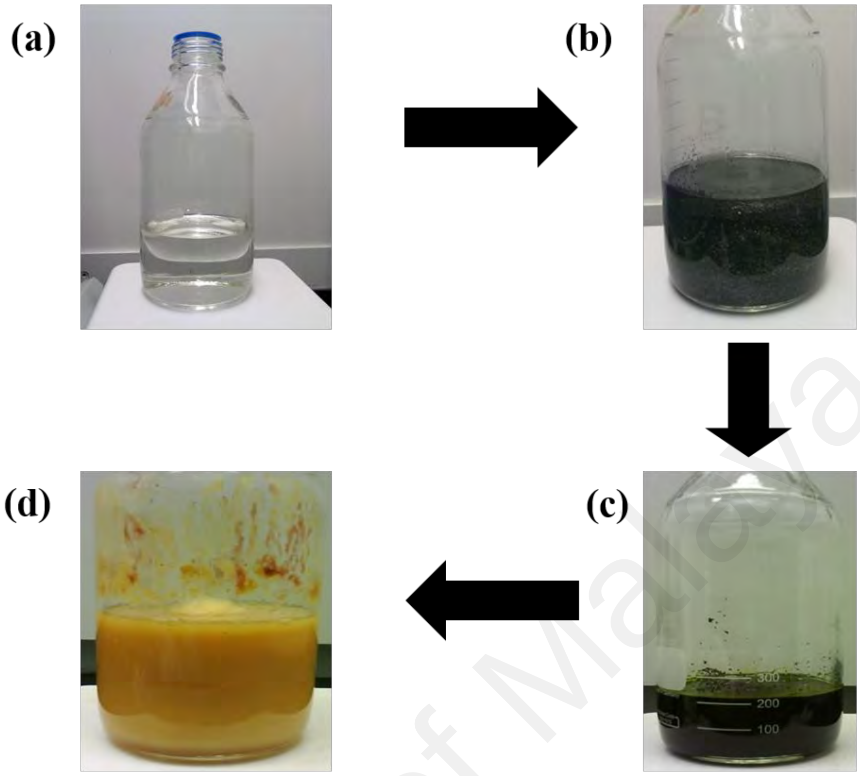

Figure 3.3: Synthesis step of GO using Hummer’s method; (a) mixture of H_2SO_4 / H_3PO_4, (b) mixture of H_2SO_4 / H_3PO_4 / Graphite flakes, (c) mixture of H_2SO_4 / H_3PO_4 / Graphite flakes / $KMnO_4$ and (d) mixture of H_2SO_4 / H_3PO_4 / Graphite flakes / $KMnO_4$ / H_2O_2.

To synthesize GO using Hummer’s method, a 9:1 mixture of H_2SO_4 / H_3PO_4 (180: 40 mL) was added into graphite flakes (1.5g) + $KMnO_4$ (9.0g). Sample was stirred for two days, then 30% H_2O_2 was poured into the sample with ice cubes. The steps of producing GO using Hummer’s method were shown in Figure 3.3. Later, samples were washed with Hydrochloric Acid (HCL) for 3 times as in Figure 3.4(a). Then, the washing process was followed with Deionized Water (DIW) for 7 times or more as shown in Figure 3.4(b). The samples were then centrifuged at 9600 rpm for 10 minutes. Then the GO is successfully produced referring to Figure 3.5(a). After drying process it became dried GO as can be seen in Figure 3.5(b).


Figure 3.4: (a) GO in HCL and (b) GO in DIW.


Figure 3.5: (a) GO and (b) Dried GO.

3.3 Solar Cell Fabrication

For solar cell device fabrication, the process required organic materials, solvents, electrodes and substrates. Chemical solutions were used as-purchased and synthesis processes were conducted accordingly in order to meet the requirements of the experiment. The substrates, electrodes preparation and cleaning processes will be explained in the sub-sections of this chapter.

3.3.1 Substrates and Electrodes

Quartz and glass substrates were used for characterization while ITO coated glass substrates were used for device fabrication of solar cells. All these substrates were cut and patterned according to the needs before the next step of washing the substrate were taken prior to device fabrication. In this work, diamond glass cutter was used to cut out the length and width of the substrates of 2.5cm x 2.0cm (length x width). All these substrates were purchased from Sands Co., Ltd. In PSC fabrication, transparent ITO and Al were used as anode and cathode electrodes, respectively. The sheet resistance of ITO coated layer side is ≈10 Ω/sq. ITO conductive electrodes have transparency of >90%, which offer excellent characteristics to be applied in PSC.

3.3.2 Substrates Patterning and Cleaning

An etching process on ITO substrates is important to get the desired pattern before those substrates are able to be used in fabricating PSC. Next, the ITO substrates need to be cleaned to remove any residual contamination on the surface of substrates. As for patterning procedure, the small area represents ITO area was covered by nail polish as can be seen in Figure 3.6 and Figure 3.7. Hydrochloric acid (HCl) solution was used to etch the remaining conductive area represents glass area at an annealing temperature of ≈ 90°C for 20 minutes until the conductive area was completely removed.

For each type of substrate, the method used for the cleaning process is different from each other. For the etched ITO substrates, acetone was used to remove the coating of nail polish. ITO substrates were immersed in acetone for 15 minutes inside the ultrasonic bath, then DIW is used to remove the acetone left over. For further cleaning process, the substrates were immersed in isopropanol. Then, once again the substrates were rinsed with DIW to remove the isopropanol left over. Finally, those substrates were dried using nitrogen gas flow.

Quartz and glass substrates cleaning method was initiated by immersing the substrates into DECON^{TM} foam solution which has been diluted with DIW. Then, the substrates were sonicated in ultrasonic bath for 15 minutes to get rid of residual contamination attached to the substrates. Later, those substrates were rinsed using DIW, followed by acetone solution, then ethanol solution. After that, those substrates were rinsed using DIW again to remove all the traces of contaminant to ensure that they were completely clean. Lastly, nitrogen gas flow was used to dry the substrates.

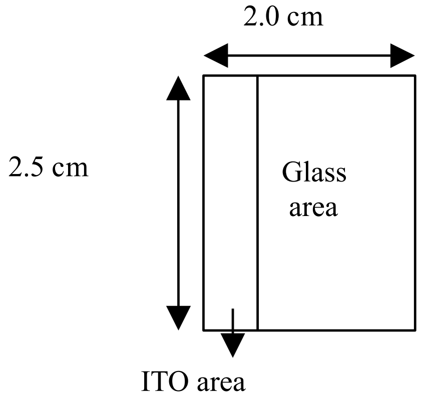

Figure 3.6: ITO substrates patterning.

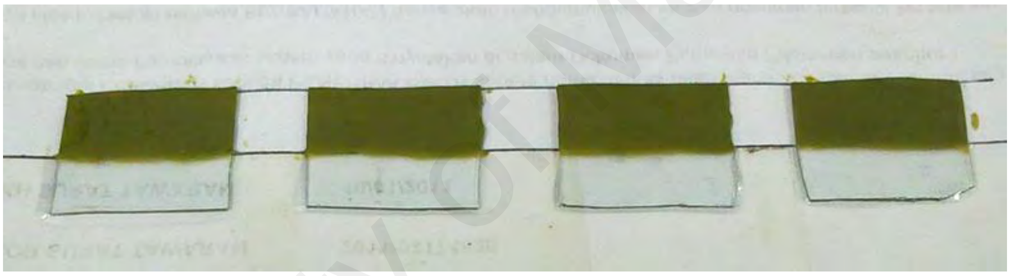

Figure 3.7: ITO substrates covered with nail polish for patterning.

3.3.3 Thin Films via Spin Coating Technique

Spin coating technique is one of the simplest and most common techniques for rapidly depositing thin coatings onto relatively flat substrates. In this experiment, SCS G3 Spin Coater was used to deposit the film layers as shown in Figure 3.8. The spin coating instrument is very important to produce uniform thin films with desired thickness. This spin coating technique is suitable for organic materials compared to thermal evaporation method since it does not require high temperature that can cause the organic materials to decompose.

Preparing thin films using spin coating technique only needs a few simple steps. It is started by placing a cleaned substrate at the centre of the disk plate. The substrate will not move and stay at the centre position as there is a small hole which serves a vacuum chuck to firmly hold the substrate. Then, a few drops of chemical solution was deposited onto the substrate. Next, switched the vacuum on and pressed start button. The disk plate started to spin at required speed and time. After it has stopped, the vacuum is switched off and the sample can be taken out of the spin coater. Later, the films were dried under room temperature for a certain time to ensure the residual solvent has been completely evaporated. Finally, this substrate was used to characterize or move to other steps of experiments.

Figure 3.8: The spin coating instrument used for thin films deposition.

3.3.4 Aluminium (Al) Electrodes Deposition via Thermal Evaporation

For PSC fabrication, the Al electrode was deposited on the active layer using an Edward 306 thermal vacuum evaporator as shown in Figure 3.9. The aluminium material was placed below the substrate coated with thin films. The temperature needs to be adjusted slowly from lower temperature until the Al was evaporated and coat the substrates through a designed mask.

3.3.5 Glovebox

Finally after process of electrode deposition, PSC devices were then under through the thermal annealing process which was conducted in the glove box. Studies showed a surface morphology change with annealing for P3HT devices (Aruna & Joseph, 2017). An annealing treatment was performed by heating the device for certain temperature and time required in a glove box. Figure 3.10 shows a glove box that has been used in this experiment.

Figure 3.9: Thermal evaporation system for Al electrode deposition.

Figure 3.10: Glove box.

3.3.6 Fabrication Procedures of PSC

In this study, fabrication of PSC will be using two types of common solar cell structure. Single layer structure was used for pristine P3HT in the active layer as can be seen in Figure 3.11 (a) while bulk heterojunction structure was used for P3HT:GS in the active layer as shown in Figure 3.11 (b).

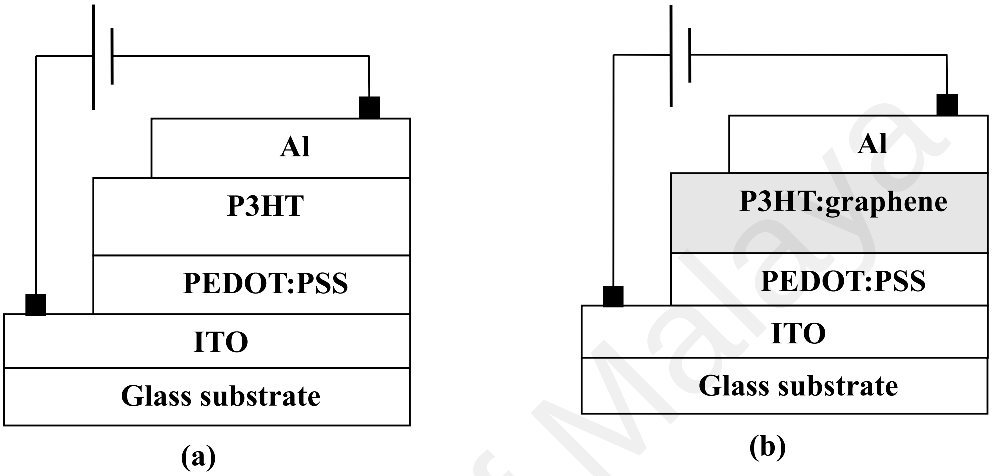

Figure 3.11: The structure of PSC (a) single layer (b) bulk heterojunction.

For the fabrication of the solar cells, poly(ethylene dioxythiophene) doped with polystyrene sulfonic acid (PEDOT:PSS) was spun coated on the ITO coated glass substrate at 3000 rpm for 30 seconds and later baked at 150 °C for 30 minutes. Next, in the active layer of PSC fabrication for BHJ structure, P3HT was mixed with GS produced by sonication process as stated previously. 20 mg of poly(3-hexylthiophene) (P3HT) (Sigma Aldrich) was added to approximately 0.5 mg of graphene in 1 ml chloroform. Then the blend solution of P3HT:GS was spin-coated on PEDOT:PSS, at 800 rpm for 30 s and dried for 30 minutes in a covered glass petri dish. The films were annealed at 130 °C for 10 minutes on a hot plate in a glovebox filled with high purity nitrogen to remove the residual solvent from the film. The top Al electrode was deposited on the active layer by thermal evaporation through a designed mask. A post-annealing treatment was performed by heating the device for 20 minutes at 120 °C in a glovebox. The chemical structures of GS and P3HT are shown in Figure 3.12 (a) while the PSC devices configuration is shown in Figure 3.12 (b).

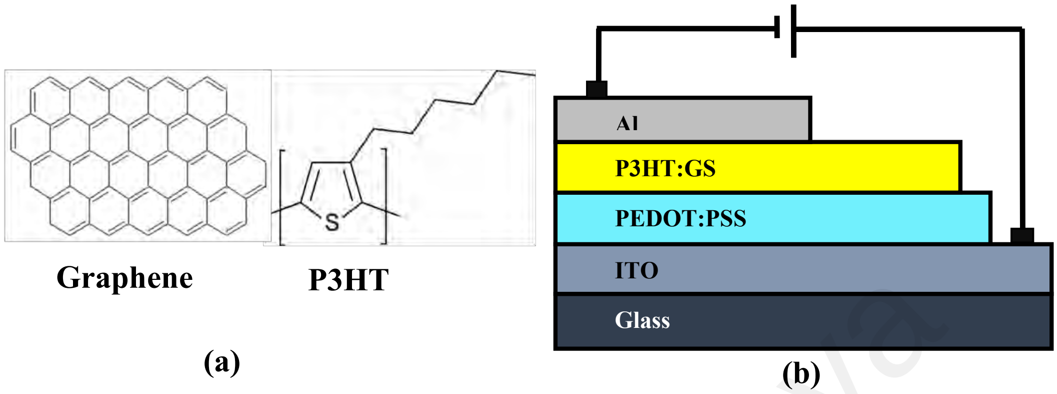

Figure 3.12: (a) The chemical structures of GS & P3HT and (b) PV device sandwiched structure.

3.4 Characterization Techniques

In this section, the experimental techniques and instruments that have been used for the characterization and investigation of the thin films and devices of PSC will be discussed in further details. All spectroscopic and microscopic measurements were performed at atmospheric pressure and room temperature.

3.4.1 Ultraviolet-Visible-Near Infrared (UV-VIS-NIR) Spectrophotometer

The absorption spectra was measured using a Jasco V-570 UV-VIS-NIR Spectrophotometer on the P3HT:graphene thin films. Ultraviolet and visible spectrometers have become one of the most important analytical instruments in the laboratory. It uses light in the visible and adjacent (near-UV and near-infrared (NIR)) ranges and beneficial to characterize the absorption, transmission, and reflectivity of variety materials. Ultraviolet (UV) and visible radiation comprise only a small part of the electromagnetic spectrum, in which the ultraviolet region falls in the range between 190-380 nm, while the visible region falls between 380-750 nm. Ultraviolet and visible radiation interacts with substance and causes progression of electrons from the ground state to a high energy state which is also referred as electronic transitions. Table 3.1 shows various spectral regions and wavelengths while Figure 3.13 shows possible electronic transitions of π, σ and n electrons. Figure 3.14 shows the Jasco V-570 UV-VIS-NIR Spectrophotometer.

Table 3.1 Various spectral regions and wavelengths.

REGION	WAVELENGTH (nm)
Far ultraviolet	10-200
Near ultraviolet	200-380
Visible	380-780
Near infrared	780-3000
Middle infrared	3000-30,000
Far infrared	30,000-300,000
Microwave	300,000-1,000,000,000

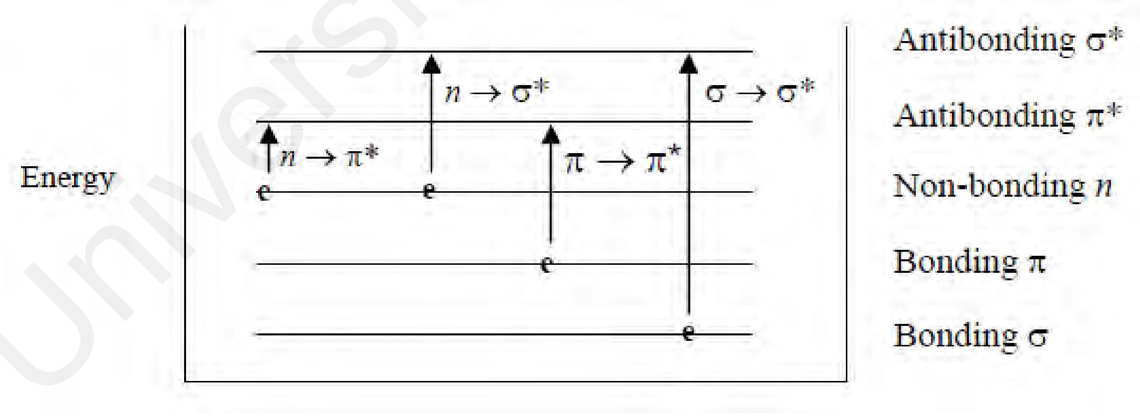

Figure 3.13: Possible electronic transitions of π, σ and n electrons (Ahmad, 2003).

Figure 3.14: Jasco V-570 UV-VIS-NIR Spectrophotometer.

3.4.2 Determination of Optical Band Gap Transition, *n* and Band Gap, E_g

One of the important parameters that govern the optical characteristics of organic semiconductor materials is the optical band gap, E_g. It is commonly used to estimate the energy separation between HOMO and LUMO of the organic semiconductor materials. According to Fujii, optical band gap, E_g can be well analyzed at the absorption edge in terms of band-to-band transition concept (Fujii et al., 1995). Absorption coefficient, α is well known to play an important role in determining the optical band gap, E_g. It can be calculated by exploiting Beer Lambert law equation:

$$I = I_0 \exp(-\alpha t) \tag{3.1}$$

In Equation 3.1, I_0 is the intensity of the incident light and t is the material thickness. The value of absorption coefficient, α is generated from $\alpha = 2.303A/t$ in where A is the absorbance intensity. By assuming that the absorption edge tends to possess a parabolic variation with the photon energy, hv, optical band gap, E_g can be estimated by the Tauc relation (Muhammad et al., 2010):

$$\alpha hv = \alpha_0 (hv - E_g)^n \tag{3.2}$$

where α_0 is the energy independent constant and n is the value to determine type of E_g transition either direct transition (n=1/2) or indirect transition for (n=2). In order to estimate n, a new equation is generated by applying the natural logarithm and the derivation of Equation 3.2. This equation is expressed as below:

$$\frac{dln(\alpha hv)}{dhv} = \frac{n}{hv - E_g} \tag{3.3}$$

This in turn will enable the generation of the plot of $dln(\alpha hv)dhv$ - hv from Equation 3.3. The peak at the particular energy value gives the approximate value of E_g where E=E_g. It is worth to note that these values are just the initial values that will be utilized for plotting a graph of ln(αhv) vs ln(hv-E_g). The slopes of the graph enable the estimation value of n. A graph of $(\alpha hv)^2$ -E is then plotted in order to evaluate the value of E_g more precisely. The extrapolated intercept of the linear portion of the graph at $(\alpha hv)^2$ = 0, yield the value for optical band gap, E_g.

3.4.3 Renishaw Raman/PL Microscope (RAMAN)

Both photoluminescence and Raman spectra were measured using a Renishaw Raman Microscope. Raman spectroscopy is a non-destructive method for obtaining valuable information about a sample's structural or chemical identity. The Raman Effect occurs when light from a strong source, typically a laser interacts with material. Most of the light is absorbed or scattered without any wavelength change (Rayleigh scattering), but some is scattered into other wavelengths, which is Raman scatter.

Photoluminescence (PL) is a process in which an incident beam or a laser produces an electronic excitation in a material which usually results in the creation of an electron-hole pair. The spectrum of the radiation emitted during the recombination of these photogenerated carriers contains information about the properties of the material. In this work, the samples were prepared by the drop casting method on a clean glass substrate. Then, the samples were characterized using Renishaw Raman Microscope linked with a 514 nm line of an argon ion laser as the excitation source at room temperature. The Raman signal was integrated over 30 seconds for each spectrum started from 200 to 3000 cm^{-1}. Figure 3.15 shows the Renishaw Raman Microscope that had been used in this experiment.

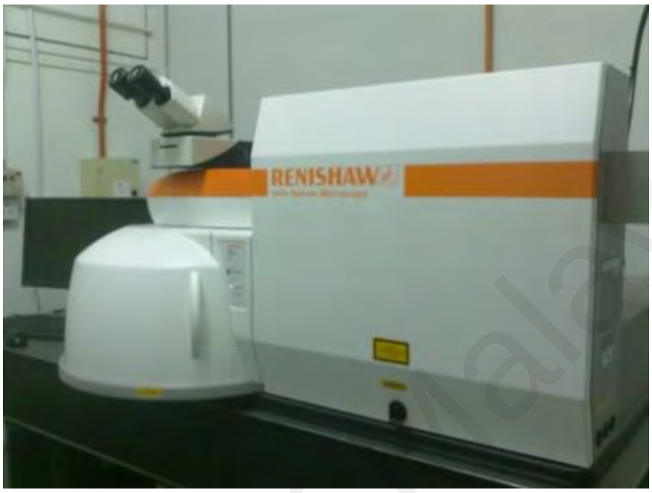

Figure 3.15: Renishaw Raman Microscope.

3.4.4 X-ray Diffraction (XRD) Technique

X-ray powder diffraction (XRD) is used for phase identification of a crystalline material and can provide information on unit cell dimensions. The properties of a material can be referred to the arrangement of atoms in its crystal structure and x-ray diffraction is a non-destructive analytical technique which can produce the unique fingerprint of Bragg reflections related to the crystal structure of the substances. In this work, the system operated at a scanning rate of 0.02^0 per second to over a 2θ range of 10^0 to 80^0. The XRD pattern of the solid powder was analyzed by Siemens D5000 (Figure 3.16) with monochromatized Cu Kα radiation and wavelength, $\lambda = 1.5418$ Å.

Figure 3.16: Siemens D5000 model XRD instrument.

3.4.5 Atomic Force Microscopy (AFM)

The atomic force microscope (AFM) is designed tool for imaging, measuring, and manipulating substances. AFM images are obtained by measurement of the force on a sharp tip (insulating or not) created by the proximity to the surface of the sample. This force is kept small and at a constant level with a feedback mechanism. When the tip is moved sideways it will follow the surface contours such as the trace *B* in Figure 3.17 (Binnig et al., 1986). In this work, the AFM measurement was carried out using tapping mode using scan size of 10.000 µm with the scan rate of 2.001 Hz Figure 3.18 shows AFM instrument model Veeco Dimension 3000 that had been used in this experiment. The measurement parameters of AFM are indicated in Table 3.2.

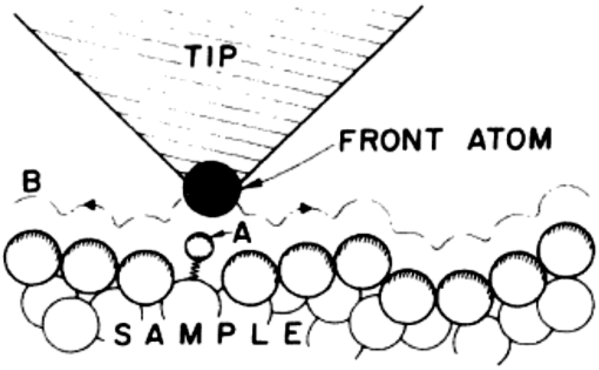

Figure 3.17: Description of the principle operation of a scanning tunneling microscope (STM) as well as that of an AFM (Binnig et al., 1986).

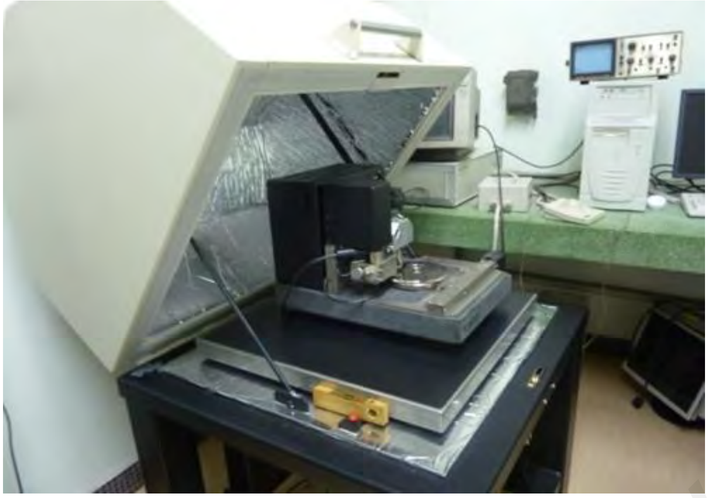

Figure 3.18: Veeco Dimension 3000 AFM instrument.

Table 3.2: Parameters of the AFM measurement.

Type	**Value**
Scan size	10.00 µm
Scan rate	2.00 Hz
Image data	Height
Data scale	10.00 nm, 250.00 nm & 500.00 nm

3.4.6 Field-Emission Scanning Electron Microscopy (FESEM)

Field-Emission Scanning Electron Microscopy is an analytical technique to analyse surface and interface conditions of electronic materials, metals, ceramics, catalysts and other substances. It is also able to analyse the existence of unknown particles on surfaces and interfaces of substances. An instrument of field-emission scanning electron microscopy is shown in Figure 3.19. FEI Quanta 400F of Field-emission scanning electron microscope (FESEM) was utilized to obtain FESEM images of the films. Samples were prepared using spin coating technique on the Si/SiO$_2$ substrate (800 rpm for 30 s). The field emission gun electron source of this model provides high current to enable imaging up to 3 nm resolution and its magnification can achieve up to 250,000 times. All the samples being tested were in thin films form.

Figure 3.19: Field-emission scanning electron microscopy (FESEM).

3.4.7 Fourier-transform infrared spectroscopy (FTIR)

The main purpose of studying the FT-IR spectrum is to identify the chemical bonding inside our material and its interaction. Infrared absorption spectroscopy is a vibrational technique used for chemical characterization of material at the molecular level. The electric dipole moments of vibrating functional groups undergo change in the infrared active transitions as they interact with the incoming infrared light. Absorptions of IR radiation by different functional groups within the sample were plotted as a function of wavelength, typically presented in units of wavenumbers or cm^{-1} (Petit & Puskar, 2018). FTIR spectroscopy was performed with Perkin Elmer Instrument FT-IR with scanning spectra recorded in the range of 400 to 4000 cm^{-1} as shown in Figure 3.20.

3.4.8 Surface Profilometer

Surface profilometer is a measuring instrument used to determine the roughness of a surface or thin film thickness. In order to define the roughness or thickness of thin films, this instrument uses a stylus to trace the cut-off length of the measured surface. In this work, samples were prepared using spin coating technique on the glass substrate (800 rpm for 30 s). Each of thin film was measured in three different spots and the average of thickness was calculated. Figure 3.21 shows an instrument of surface profilometer. The parameters used for the film thickness measurement are listed in Table 3.3.

Figure 3.20: Perkin Elmer Instrument FT-IR.

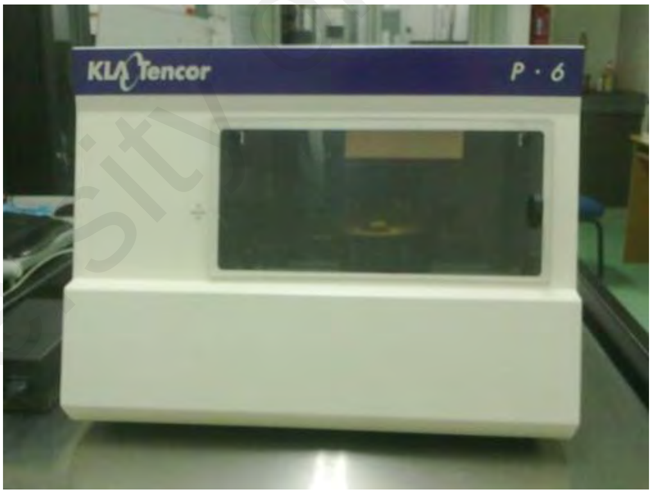

Figure 3.21: KLA Tensor P-6 surface profilometer.

Table 3.3: Scanning parameters of film thickness measurement.

Type	Value
Scan type	2D
Scan length	1000 µm
Scan speed	100 µmsec^{-1}
Sampling rate	20 Hz
Applied force	1.00 mg

3.4.9 Photovoltaic (PV) Measurement

For PV measurement, a solar simulator that had been used was Keithley 236 Source Measurement Units (SMUs) under AM1.5 G-filtered white light irradiation with power intensity of 100 mWcm^{-2} from Oriel 67005. This solar simulator is able to provide illumination that is approximately identical to the natural light which is important to identify the efficiency of the fabricated PSC. For this experiment, the scan range used are from -2.5 V to 2.5 V while the scan rate is 0.125 V/s. Figure 3.22 below shows the solar simulator instrument used in this experiment.

Figure 3.22: A Keithley 236 SMU instrument.

The electrical measurement will be performed on the devices in air using a Keithley 236 source measurement units, and an Oriel Xenon with an AM1.5 filter as the light source with an intensity of 100 mW cm^{-2}. The PV properties of short circuit current density (J_{sc}), open circuit voltage (V_{oc}), and solar power conversion efficiency were obtained.

CHAPTER 4: GRAPHENE SHEETS AND GRAPHENE OXIDE; SYNTHESIS, CHARACTERIZATIONS, AND SOLUBILITY IN ORGANIC SOLVENTS

4.1 Overview

In this work, graphite flakes are used as the precursors for synthesizing Graphene Sheets (GS) and Graphene Oxide (GO), where they undergoe direct exfoliation and oxidation process using simplified Hummers' method to produce GS and GO, respectively. The results from the characterization of the materials including UV-Vis, FTIR, FESEM, as well as PL-Raman Spectrometer are presented in the sub-topic in each part.

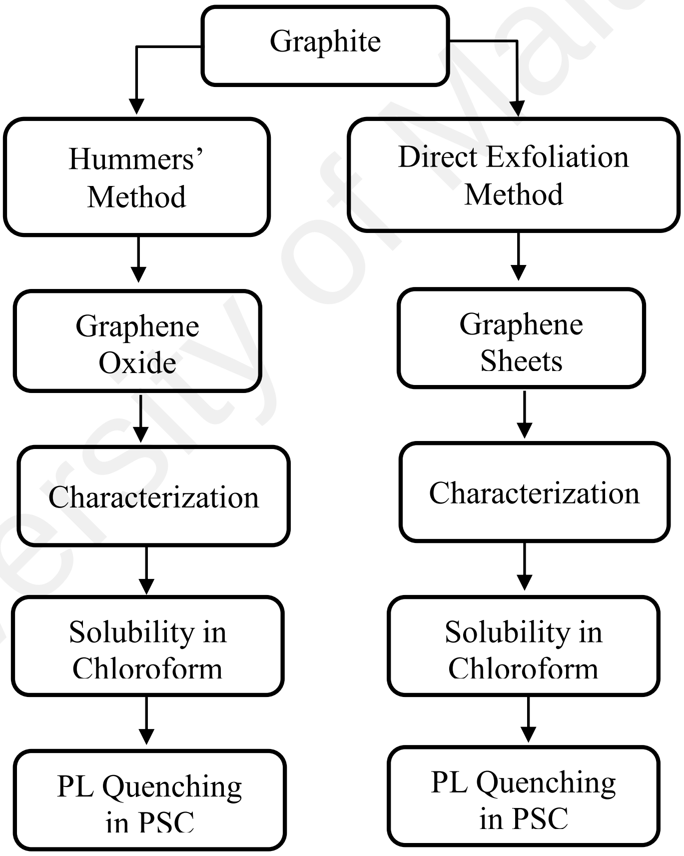

Figure 4.1: Graphic summaries of GS and GO synthesis methods used in this work.

In order to achieve a good result in PSC devices, it is very important to ensure the material we use is soluble in organic solvent. Some of the trial methods that have been done to test the solubility of the synthesized materials in the organic solvents are briefly discussed at the end of each part. The first part of this chapter will discuss about direct exfoliation of graphite in chloroform to obtain GS using ultrasonication technique. The second part of Chapter 4 focuses on the synthesis of GO using simplified Hummers' method. Figure 4.1 displays the flowchart of the research work to give a brief understanding on how the works are conducted.

4.2 Graphene Sheets (GS)

4.2.1 Synthesis of Graphene Sheets Using Exfoliation Method

In this study, GS is obtained by exfoliation method in which 200 mg of graphite flakes are added into 10 mL of chloroform solution and undergo exfoliation using bath sonication technique. The sonication times are varied at the time of 1.5, 3, and 6 hours. In order to get a thin sheet of GS, the final solution is centrifuged at 400 rpm for 20 minutes. The supernatant of the solution is then separated from the precipitate and further used for characterizations. According to the Figure 4.2, it can be seen that 6 hours of sonication time is resulted the best concentration of GS. Nevertheless, to confirm the best concentration of GS in each vial, the concentrations of GS in these vials are calculated. The results of calculated concentration for each GS are shown in the Table 4.1.

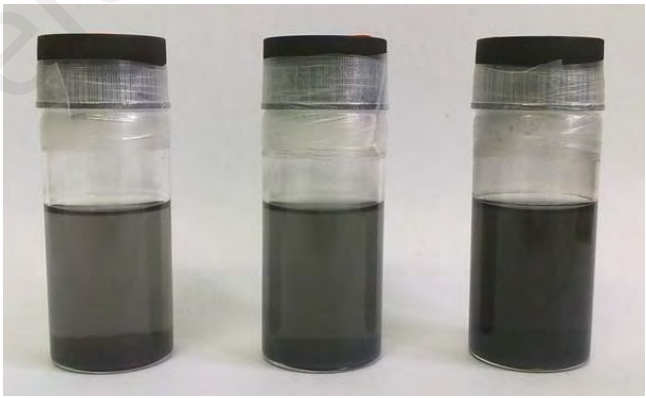

(a) **(b)** **(c)**

Figure 4.2: Supernatant GS obtained after (a) 1.5 hours, (b) 3 hours, and (c) 6 hours of sonication treatment.

By utilizing a facile exfoliation method, the homogenous and soluble GS in chloroform is obtained as shown in the photograph image of Figure 4.2. The dispersions of GS have grey to black colour liquids and are found to be stable for about two weeks in the vial. The ability of this GS to maintain stable in a vial such for some time indicates that it is dispersed well in organic solvent. As in the table above, GS obtained through sonication time of 6 hours has the highest concentration and the most stable during observation. This is a good sign to prove that exfoliation method via sonication process is one of the simple ways to obtain exfoliated GS in organic solvent without the need to cooperate with any other chemicals.

Table 4.1 Value of GS concentration with different sonication times.

Samples	Sonication time (hours)	Concentration (mg/ml)
(a) GS (1.5 hours)	1.5	≈ 0.01
(b) GS (3 hours)	3.0	≈ 0.02
(c) GS (6 hours)	6.0	≈ 0.5

4.2.2 Characterization of Graphene Sheets

After the exfoliation method via sonication process of graphite, the obtained GS can be visualized in the FESEM image of Figure 4.3. As we can see from the FESEM image, the GS formed are semi-transparent which indicates that a few thin layers of GS have been formed. It is worth noting that GS have a sheet-like structure with smooth surface and possess an average lateral dimension of about 2 μm. Exfoliation of graphite via sonication process has proved that this method is capable to disperse GS well in organic solvent using a facile way.

Next, the GS is characterized using PL-Raman spectroscopy to investigate the layer of GS that has been formed. The number of GS layer plays an important role to provide good results when used as material in the experiment. The GS should be very thin and have no excessive layers that can reduce its benefits. It is known that single and bilayer GS have many interesting properties to be explored. The GS in this experiment consist of multiple layers of graphene, as indicated in the Raman spectra shown in Figure 4.4. Usually for Raman spectra of single-layer graphene, G peak appeared at 1580 cm^{-1}, D peak at 1350 cm^{-1} and 2D peak at 2680 cm^{-1} (Elias et al., 2009). There are three Raman peaks occur at 1353 cm^{-1}, 1582 cm^{-1} and 2720 cm^{-1}, which correspond to a D-band, G-band and 2D-band, respectively.

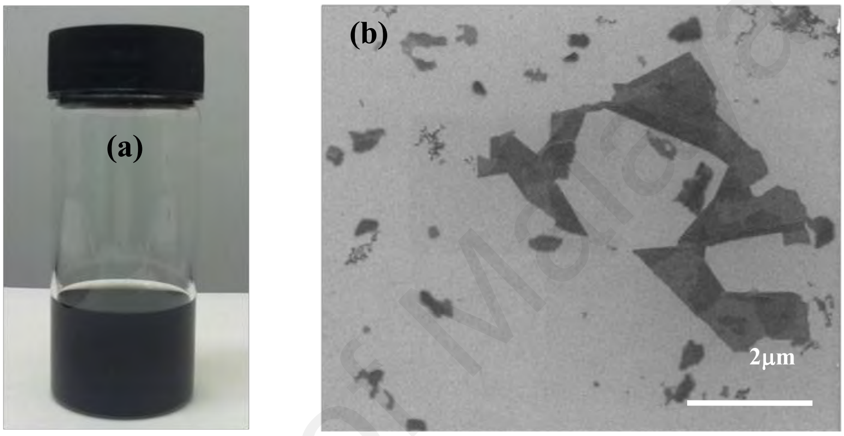

Figure 4.3: Supernatant GS in chloroform and (b) FESEM image of the GS after sonication process. The sample was prepared by spin coating (3000 rpm, 30 sec) on silicon substrate.

According to Ferrari *et al.*, the number of layers for n-layer graphene can be measured by observing the shift and shape of the 2D peak (Ferrari et al., 2006). From the results, it can be seen that the 2D peak of GS appeared at 2720 cm^{-1}, shifts to the higher wavenumber and becomes broader compared to single layer graphene (2D:2680 cm^{-1}). This behaviour confirms the presence of multiple layers of the produced GS via a simple exfoliation process. It is reported that a few layer (<10 layers) of graphene materials also have interesting properties as they still exhibit two dimensional properties (Geim & Novoselov, 2007) compared to the single and bilayer graphene. This means the GS obtained from exfoliation of graphite via sonication process is suitable to be applied in various applications.

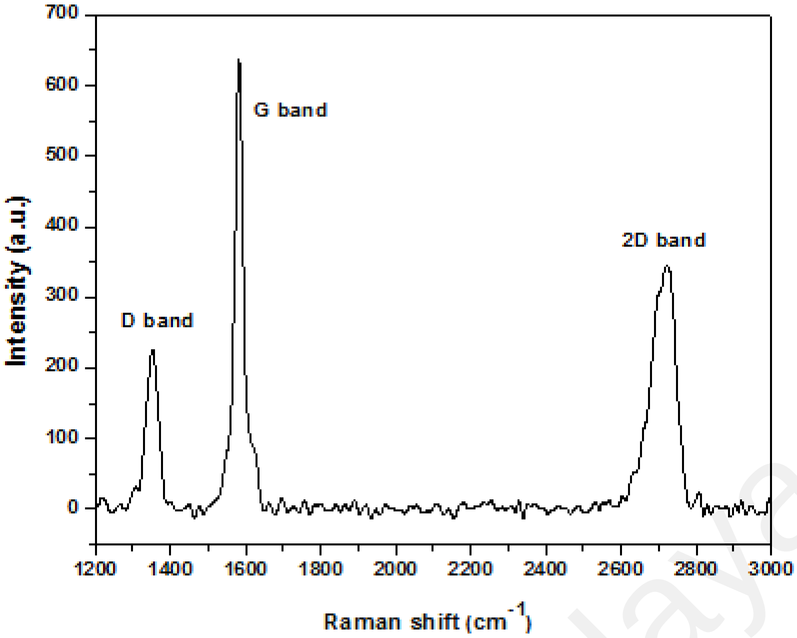

Figure 4.4: Raman spectra of GS thin films.

4.2.3 Solubility of Graphene Sheets in Organic Solvent

GS obtained from exfoliation method, as can be seen in Figure 4.5(a) is mixed with P3HT pristine solution in Figure 4.5(b) and continuously stirred for 24 hours under the room temperature to produce a well blend mixture of P3HT:GS as shown in Figure 4.5(c). As can be seen, the mixture of GS and P3HT pristine solution form a homogenous and stable solution, demonstrate a successful blending between both materials.

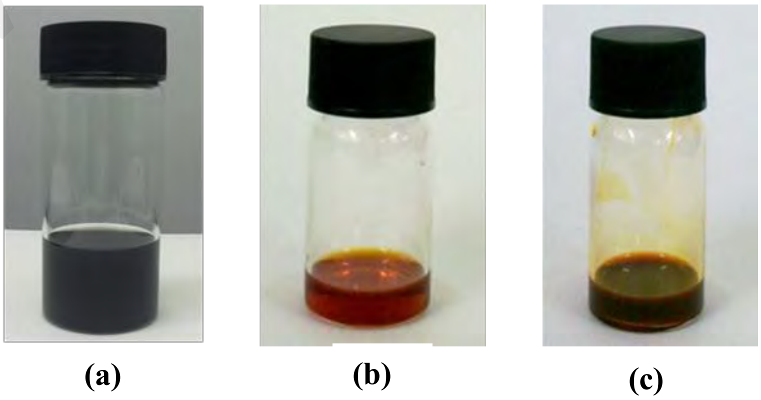

(a) **(b)** **(c)**

Figure 4.5: The photograph of (a) GS, (b) P3HT and (c) P3HT:GS solutions.

4.2.4 PL Quenching for Polymer Solas Cell Fabrication

In order to get good results in fabricating the PSC, it is important to conduct the photoluminescence (PL) characterization in order to have an early expectation of fabricated solar cells devices. Quenching effect is one of the important characteristic to predict the outcome of the solar cells. This is a crucial part before PSC devices can be prepared for electrical characterization. No quenching effect occurs in the PL spectrum will bring a meaning of there is no exciton dissociation within active layer, hence the efficiency of PSCs will be decreased. If the mixture materials show disappointing result, therefore it is incompetent to be used as an acceptor in PSC.

Figure 4.6 demonstrates the PL spectrum of the P3HT:GS blend and pristine P3HT films on glass substrates. The maximum PL peak for P3HT and P3HT:GS is observed at the same position (710 nm) but with different intensity. The PL intensity is decreased to some extent, upon the addition of 2.5% of GS in P3HT. The reduction in the PL intensity is so-called PL quenching, indicates an efficient charge transfer between P3HT and GS (Xu & Holdcroft, 1993). This result implies that GS may act as an electron acceptor material for polymer-based solar cell applications, therefore this sample will be used for further study of this work. Other researchers also observed similar PL quenching behavior, e. g., in a functionalized graphene:P3HT blend (Liu et al. 2010). The values of average thickness for pristine P3HT and P3HT:GS blend films are tabulated in Table 4.2.

4.3 Graphene Oxide (GO)

4.3.1 Characterization of Graphene Oxide

In order to determine the optical properties of GO, ultraviolet-visible-near infrared (UV-Vis-NIR) absorption spectra measurement has been carried out. The absorption spectra of GO is shown in Figure 4.7. From the UV-vis spectrum, two signature peaks of GO can be observed where a strong peak at 230 nm is related to the π→π* transitions of aromatic C-C bonds while a shoulder at about 300 nm corresponds to the n→π* transition of C=O bonds (carbonyl groups). The peaks obtained from this synthesized GO is consistent with the literature review (Lai et al., 2012), thus confirm the formation of GO after Hummers' method.

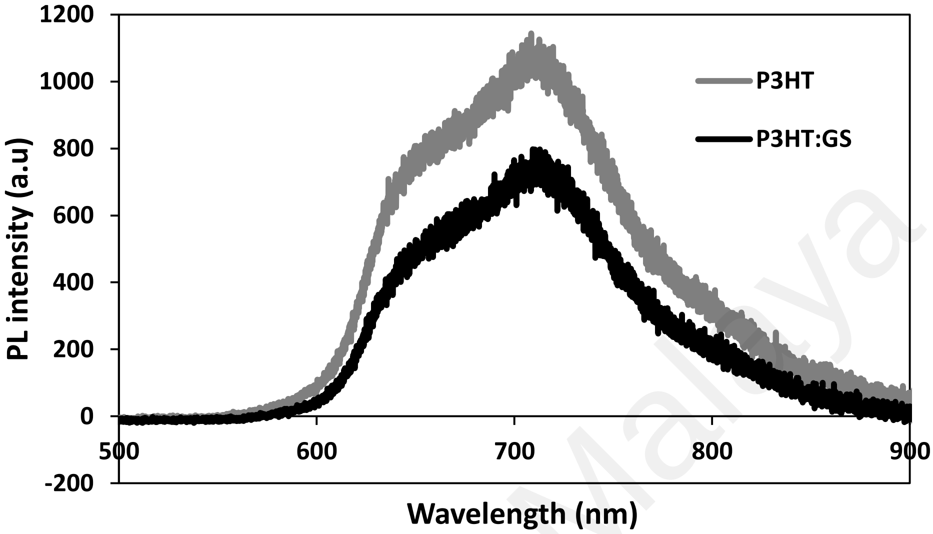

Figure 4.6: PL spectra of P3HT and P3HT:GS blend thin films using exfoliation method.

Table 4.2 The values of average thickness for pristine P3HT and P3HT:GS blend films.

Samples	**Film thickness**			
	Spot 1	**Spot 2**	**Spot 3**	**Average thickness (nm)**
Pristine P3HT	122.6	125.4	123.2	123.7 ± 0.1
P3HT:GS	127.2	124.3	125.5	125.7 ± 0.1

Next, Fourier-transform infrared spectroscopy (FTIR) has been employed in order to analyze the attachment of chemical compound to GO. Figure 4.8 depicts the FTIR spectrum of GO scanned in the range of 500 to 3800 nm where four prominent peaks can be seen. The peaks appeared at position around 3446 cm^{-1}, 1631 cm^{-1} and 1400 cm^{-1} can be assigned to the O-H stretching and bending vibration, thus show the intercalated free H_2O molecules on GO (Pham et al., 2011). In spite of the intercalation of water molecules, the peak at 1631 cm^{-1} may also be attributed to the C=O bands, which suggests the presence of carboxylic acid and carbonyl moieties along the sheet edges and basal plane of GO (Ossonon & Bélanger, 2017a, 2017b). The peak at 1044 cm^{-1} determined C-O stretching vibration of alkoxy group which further confirms the presence of oxygen containing functional group within the GO structure (Bera et al., 2018).

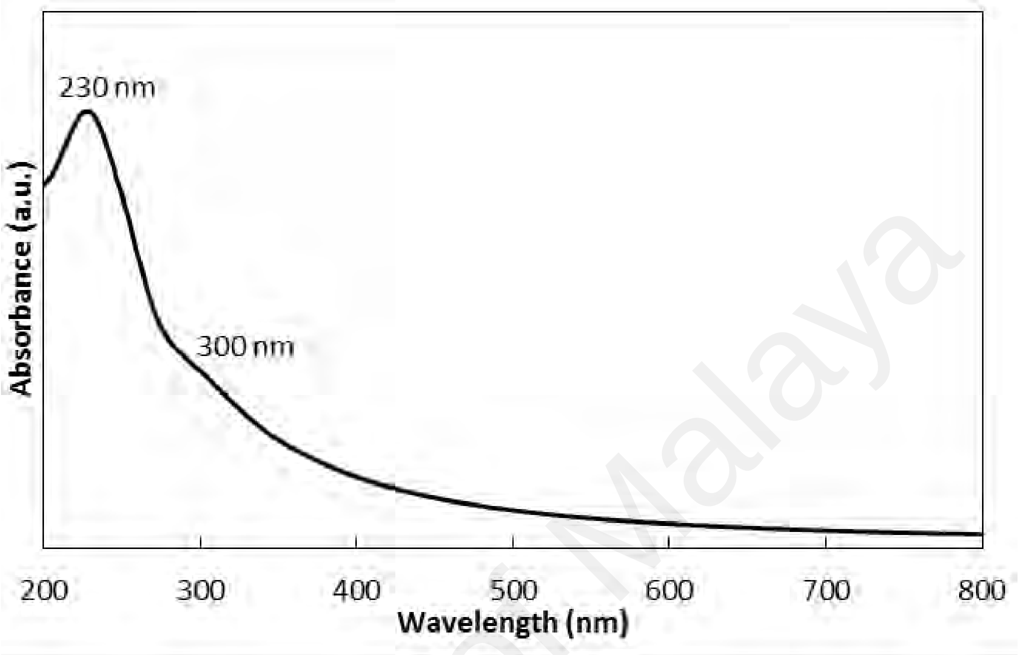

Figure 4.7: UV-Vis-NIR spectrum of GO obtained after Hummers' method.

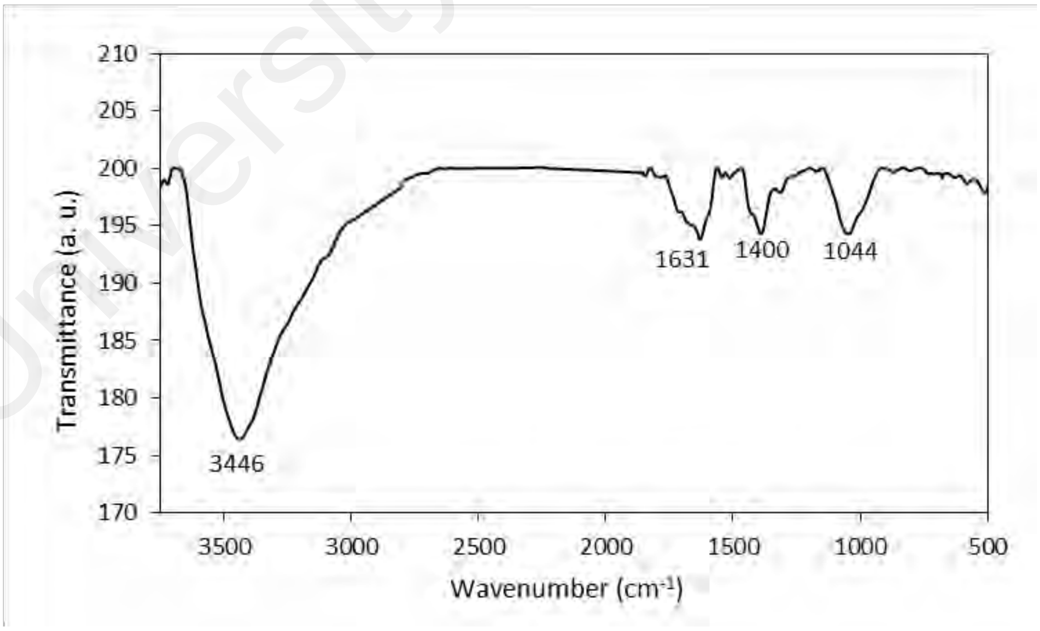

Figure 4.8: FTIR spectrum of GO scanned in the range of 500 to 3800 nm.

To determine the structural property of GO, the X-ray diffraction (XRD) measurement has been carried out. Figure 4.9 shows the XRD spectrum of GO in powder form within the angle 2θ ranges between 10° and 80°. The XRD spectrum exhibited a strong diffraction peak at scattering angle (2θ) of about 11° corresponded to the (002) plane of GO (Naebe et al., 2014). The separation distance between the lattice plane or well-known as d-spacing corresponding to the strongest peak at crystallographic plane (002) of GO is determined and found to be 0.82 ± 0.01 nm by applying Bragg's equation:

$$n\lambda = 2d\sin\theta \tag{4.1}$$

where n is an integer representing the order of XRD diffraction peak, d is the spacing distance between the lattice planes, θ is the Bragg diffraction angle, and λ is the wavelength of the X-ray radiation source (here, Cu Kα radiation of 0.154 nm is used). The high value of d-spacing indicates the presence of oxygen-rich groups (carboxylic acid, carbonyl, hydroxyl and epoxy groups) on both sides of the GO sheets as well as trapping of water molecules between the sheets after the oxidation and exfoliation process of graphite flakes (Ma et al., 2017).

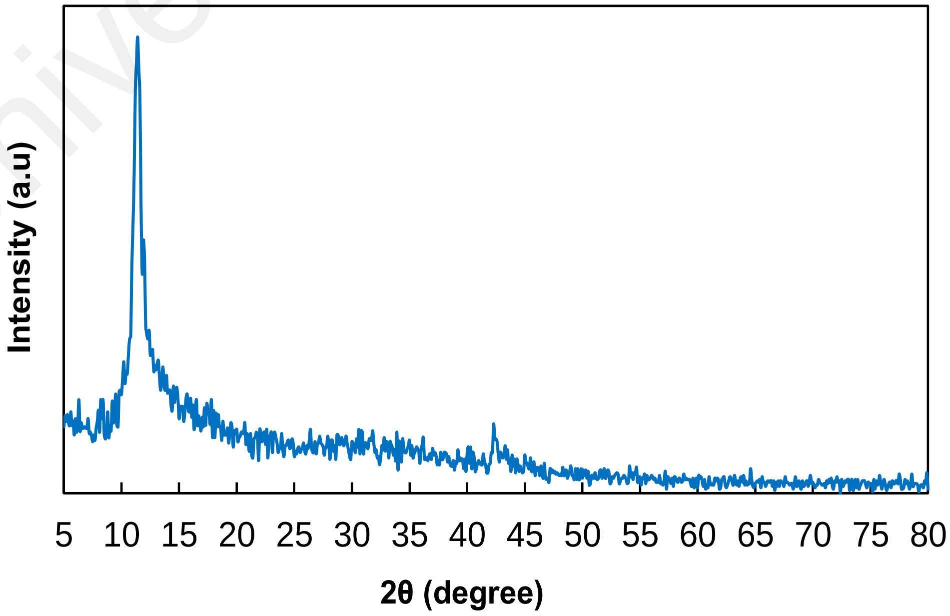

Figure 4.9: The XRD diffraction for GO in powder form.

Figure 4.10 shows the typical FESEM images of GO and sonicated GO sheets obtained by Hummers' method. As can be seen in Figure 4.10(a), the GO shows a sheet-like structure with a large surface area and few wrinkles on the surface. The presence of the wavy wrinkles on the surface of GO sheets can be attributed to the disruption of the planar sp^2 carbon sheets by the introduction of sp^3-hybridized carbon upon oxidation (Wang et al., 2009). Besides that, this result on the morphology of GO may also suggest the presence of residual H_2O molecules tightly bound with carboxyl or hydroxyl group of GO (Ju et al., 2010). Some of the GO sheets tend to break into smaller sheets upon the sonication process, as depicted in Figure 4.10(b).

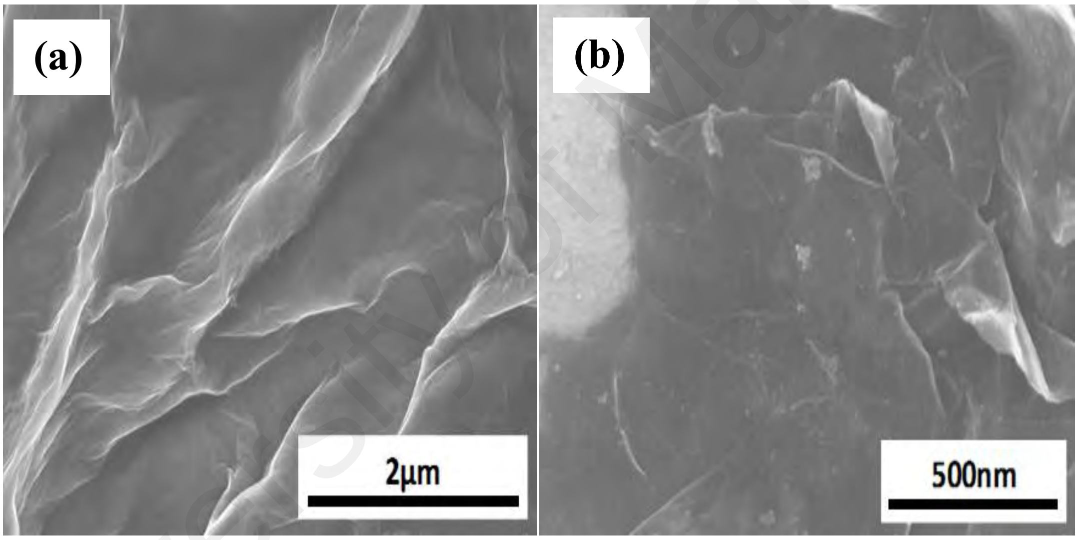

Figure 4.10: The FESEM images of (a) GO and (b) sonicated GO.

The Raman spectrum of synthesized GO is depicted in Figure 4.11 where three characteristic main peaks can be observed at 1351 cm^{-1}, 1587 cm^{-1}, and 2691 cm^{-1} which correspond to the D, G, and 2D band, respectively. It is well known that the D peak refers to the defects and disorder-activated Raman mode arise from the vibrations of sp^3 carbon atoms and the G peak is ascribed to the sp^2 hybridized carbon atoms in a graphitic 2D hexagonal lattice (Ferrari et al., 2006). Meanwhile, the characteristics of 2D band from Raman spectroscopy is used to evaluate the multilayer stacking of graphene sheets (Rajagopalan & Chung, 2014). The obtained broad 2D peak suggests that the GO consist of multiple layers of graphene. Moreover, the intensity ratio between D and G peaks gives the measure of the degree of oxidation and reduction as well as the disorder present within graphene. In this work, the I_D/I_G (2200/25000) ratio of GO was calculated to be 0.88. This ratio is consistent with the value reported by Kim et al. (2013).

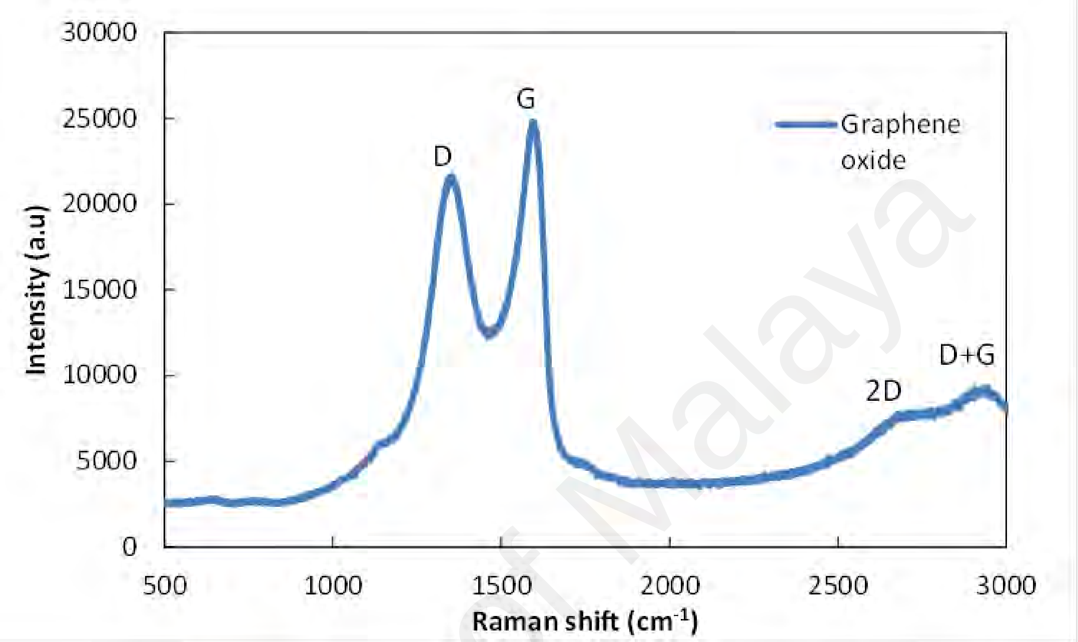

Figure 4.11: The Raman spectrum of GO obtained in the range of 500 to 3000 cm^{-1}.

4.3.2 Solubility of Graphene Oxide in Organic Solvent

A lot of trial methods have been done in order to increase the solubility of GO in organic solvents. In a typical procedure, the poly(3-hexylthiophene) (P3HT) solution (Figure 4.12(a)) is mixed with GO solution (Figure 4.12(b)) produced by the Hummer's method via simple stirring method under room temperature for 24 hours. Prior mixing with GO, P3HT powder is dissolved in 1 mL of chloroform solvent. Figure 4.12(c) shows the mixed solution of P3HT and GO in chloroform solvent.

4.3.3 PL Quenching for Polymer Solar Cell Fabrication

As we can see in Figure 4.13, there is no quenching occurred in the PL spectrum obtained from P3HT:GO solution as the PL intensity for P3HT:GO is higher than P3HT itself. This result suggests that there is no efficient charge transfer between two materials, thus the P3HT:GO blend thin film is not suitable for PSC device fabrication. The values of average thickness for pristine P3HT and P3HT:GO blend films are tabulated in Table 4.3.

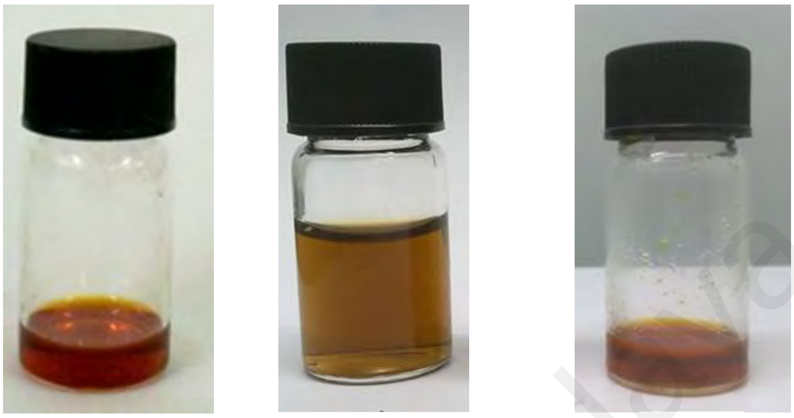

(a) (b) (c)

Figure 4.12: The photograph of (a) P3HT, (b) GO, and (c) P3HT:GO solutions.

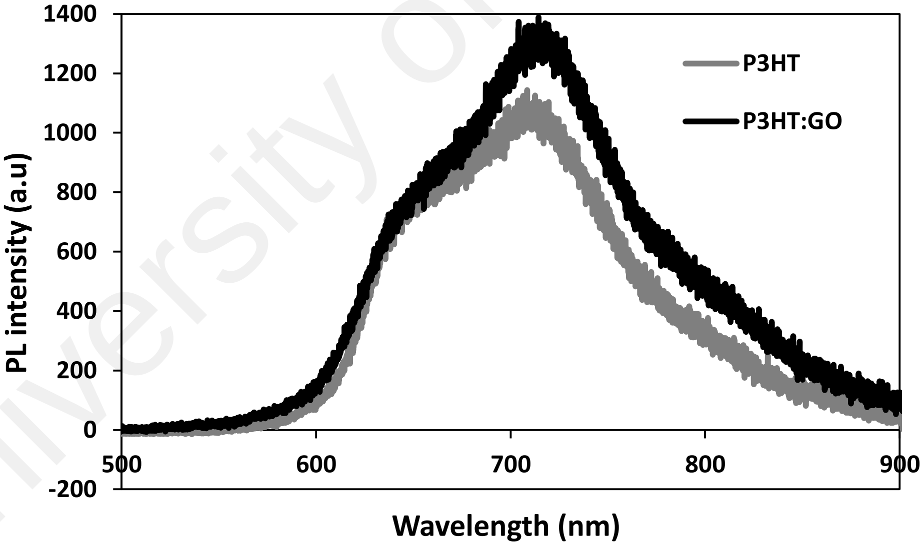

Figure 4.13: PL spectra of P3HT and P3HT:GO blend thin films from Hummers' method.

Table 4.3 The values of average thickness for pristine P3HT and P3HT:GO blend films.

Samples	**Film thickness**			
	Spot 1	**Spot 2**	**Spot 3**	**Average thickness (nm)**
Pristine P3HT	122.6	125.4	123.2	123.7 ± 0.1
P3HT:GO	124.5	126.4	127.1	126.0 ± 0.1

4.4 Summary

In order to validate PSC will get good results, PL quenching appear to be a crucial indication of the measure of success of exciton dissociation in P3HT materials based on the plenty of the report found in the literature (Kabongo et al., 2016). The quenching of P3HT emission signifies effective enhanced exciton dissociation at the interface between P3HT and GS. As we can see in this chapter, GS produced using a facile exfoliation method via sonication of graphite shows a good result to be used as an acceptor in PSC after it has been mixed with P3HT. However, GO produced using Hummer's method in organic solvents mixed with P3HT shows unsatisfactory results for PL quenching. Generally, PL quenching is an important indication of efficient charge transfer induced by the acceptor (GS) dispersed in the donor host matrix (P3HT).

CHAPTER 5: P3HT:GRAPHENE SHEETS AS AN ACTIVE LAYER IN POLYMER SOLAR CELL DEVICES

5.1 Overview

GS that has been successfully synthesized via sonication process in Chapter 4 and mixed with P3HT will be used as an acceptor to study the performance of PSC. Finally the efficiency of GS based PSC device is presented and discussed.

5.2 Solar Cell Fabrication Process

Solar cell fabrication started with the preparation of P3HT:GS blending solution for active layer. Then, the normal fabrication method using spin-coating and thermal evaporation for cathode is carried out.

5.2.1 Graphene Sheets in Polymer Solar Cell

In order to increase the device efficiency, GS which is self-synthesized using sonication process is incorporated with P3HT as the active layer of PSC. Table 5.1 shows P3HT:GS samples with different sonification times and the percentage of GS at the end of sonification process. The longer the sonification time, the higher the percentage of GS in the solution. It can be seen that the percentage of GS for 1 hour of sonication and 3 hours of sonication are too small to be significant. Meanwhile, the percentage of GS for 6 hours of sonication is an appropriate amount to study the effects of GS in PSC. Thus, P3H:GS blending solution is sonicated for 6 hours prior to the fabrication process.

Table 5.1 Percentage of GS synthesized in P3HT:GS PSC.

Samples	P3HT (g)	Graphene synthesized (g)	Percentage (%)
P3HT + GS (1h)	20	≈ 0.01	0.05
P3HT + GS (3hrs)	20	≈ 0.02	0.1
P3HT + GS (6hrs)	20	≈ 0.50	2.5

5.3 Results and Discussion

This section starts with the optical characteristic including the morphology of the active film will be discussed using PL spectra, AFM and FESEM results. The electrical characterization for the device fabricated will be presented afterwards.

5.3.1 Absorbance and Energy Band Gap

Figure 5.1 shows the absorption spectra of P3HT and P3HT:GS thin films. It can be observed that P3HT and P3HT:GS exhibit a peak maximum at 514 nm in the range of 400 – 630 nm. Upon adding GS into P3HT, there is no significant shift in absorption spectrum. This behavior may attribute to the absence of ground state interaction between two materials. However, there is a slight increase in the absorption intensity for P3HT:GS film, which implies that P3HT:GS has higher potential to absorb more light and might increase the charge generation compared to pristine P3HT.

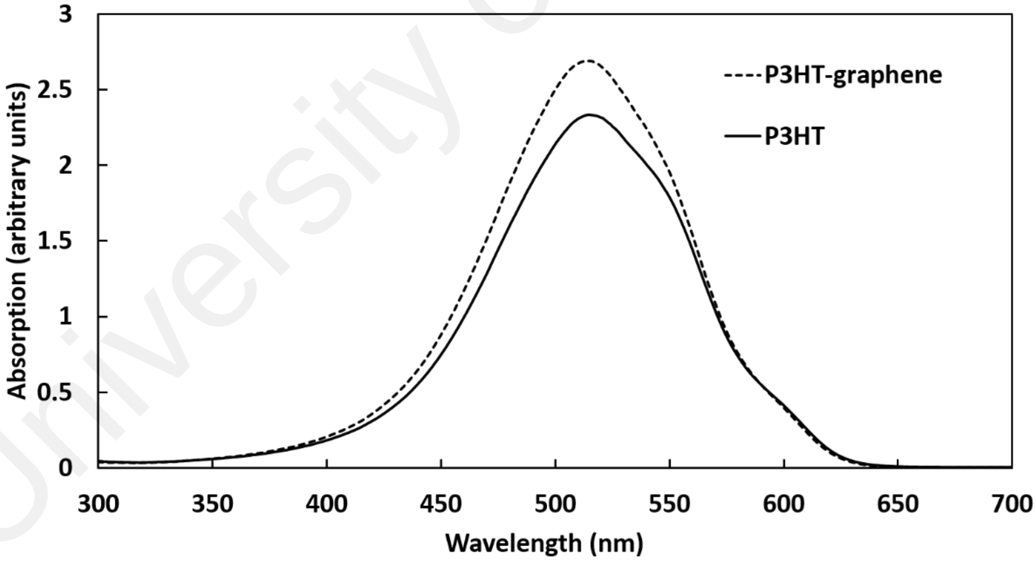

Figure 5.1: Absorption spectra of P3HT and P3HT:GS using exfoliation method.

One of the important parameters that govern the optical characteristics of organic semiconductor materials is the optical band gap, E_{g}. It is commonly used to estimate the energy separation between HOMO and LUMO of the organic semiconductor materials.

Figure 5.2 shows the typical energy band diagram for P3HT and GS. It is shown that P3HT exhibits E_g of 2.9 eV.

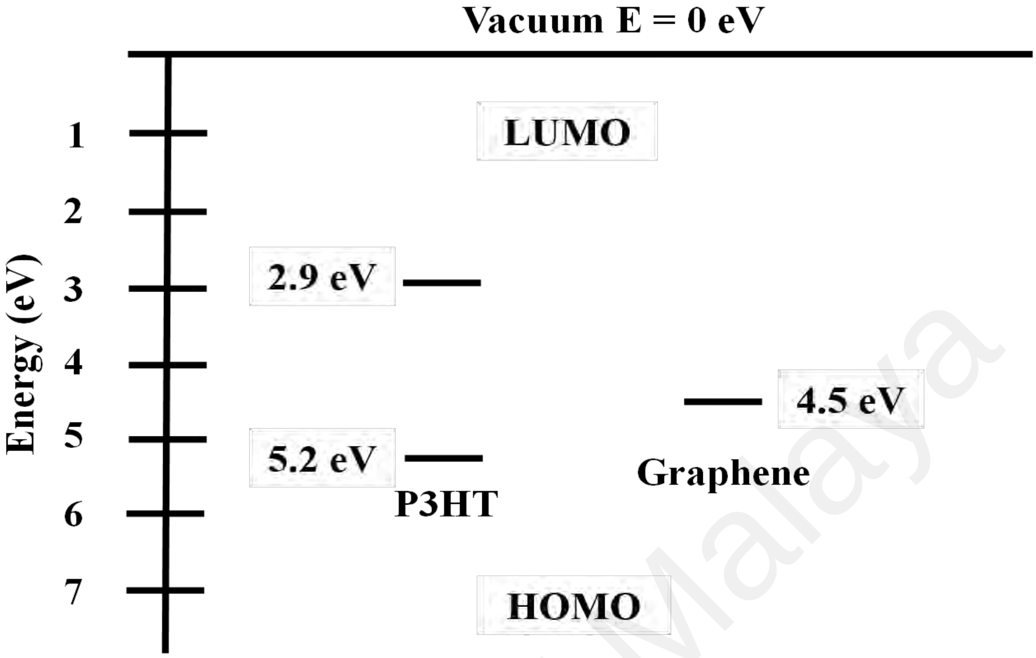

Figure 5.2: The typical energy band diagram of P3HT and graphene.

Figure 5.3 and Figure 5.4 show the plots of $(\alpha E)^2$ against E for pristine P3HT and P3HT:GS. The approximate value of the optical band gap can be seen at the slope of plot at a particular energy value where $hv = E_g$. The slope of pristine P3HT can be observed in Figure 5.5 which occurs around at $hv = E_g$ of ~ 2.15 eV while the slope of P3HT:GS can be observed in Figure 5.6 which occurs slightly closed at $hv = E_g$ of ~2.14. The results show that the value of E_g is reduced upon the incorporation of GS into P3HT which is in accordance with few other reports related to narrow bandgap for PSC (Brebels et al., 2018; Wang et al., 2019). The reduction of the band gap specifies a broader absorption spectrum has been reached whereby more photons throughout the entire solar spectrum can be harvested. These results can be further supported by the results of absorption coefficient spectra shown in Figure 5.1.

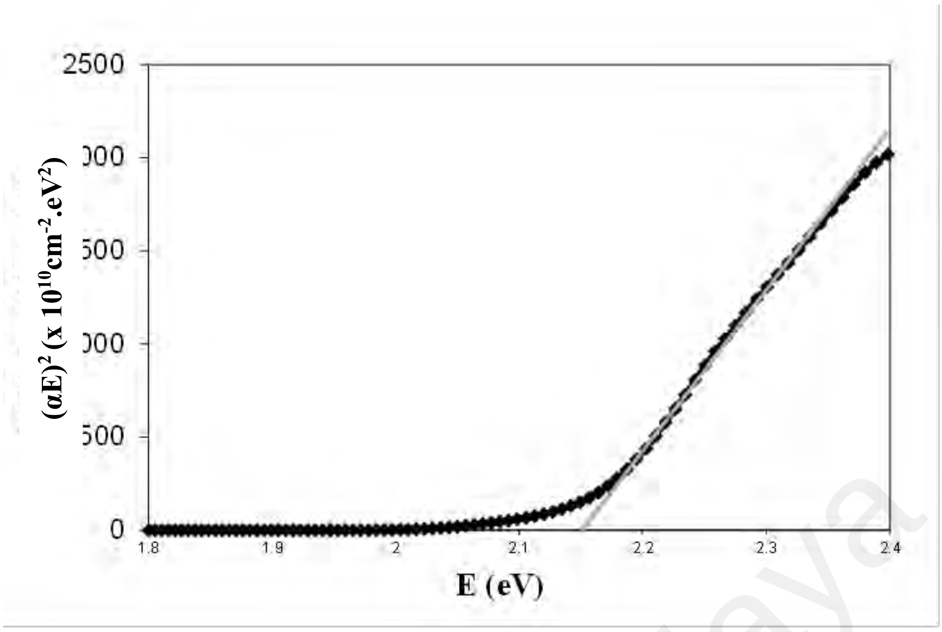

Figure 5.3: Plots of $(\alpha E)^2$ against *E* for pristine P3HT film.

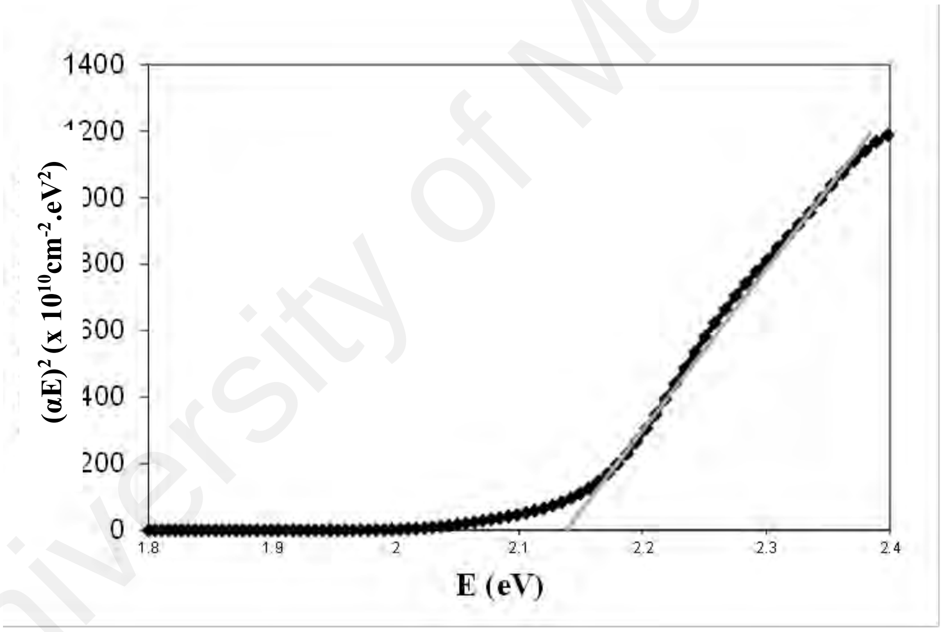

Figure 5.4: Plots of $(\alpha E)^2$ against *E* for P3HT:GS blend film.

5.3.2 Morphology Characterization

The morphology of the photoactive layer is a very important parameter which determines the photovoltaic performance of PSC (Li et al., 2005; Ma et al., 2005). In order to characterize the morphology of GS and P3HT blends, field-emission scanning electron microscopy (FESEM) and atomic force microscopy (AFM) are carried out.

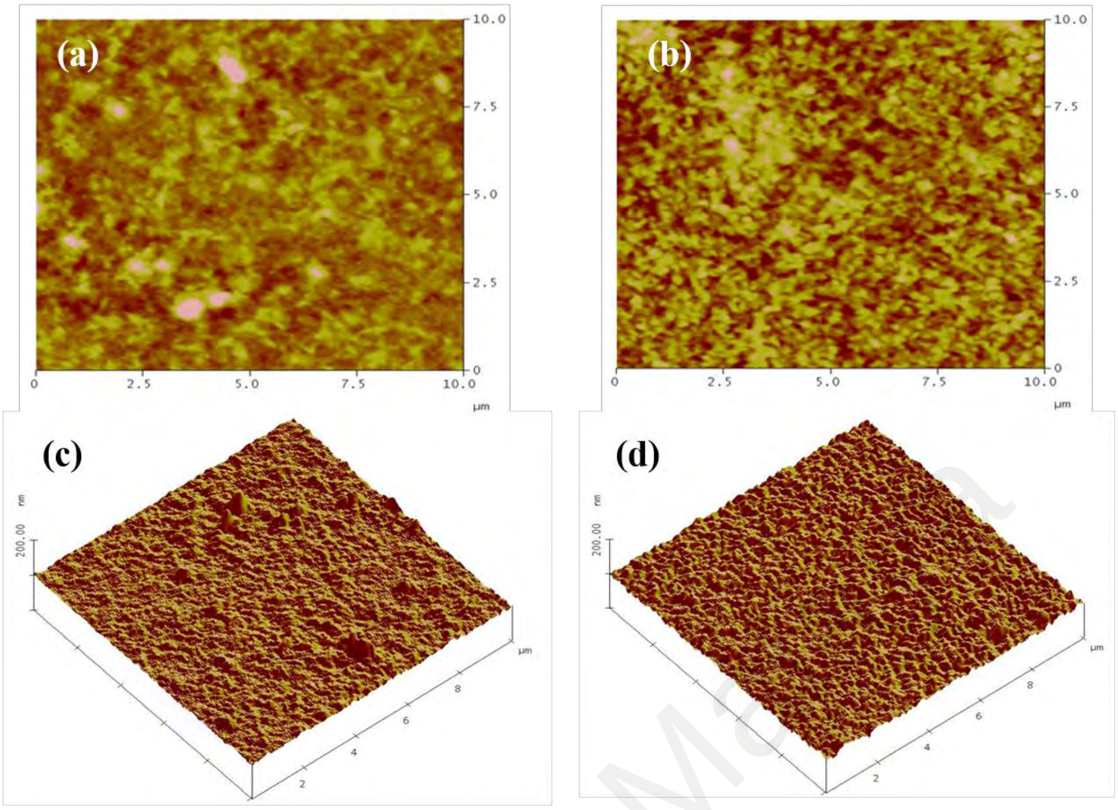

Figure 5.5: 2D AFM images of (a) P3HT & (b) P3HT:GS thin films and 3D AFM images of (c) P3HT & (d) P3HT:GS thin films.

Contact mode of atomic force microscopy (AFM) images of the P3HT and P3HT:GS blend films are shown in Figure 5.5(a) and (b), respectively. From the AFM analysis, P3HT:GS film shows a homogenous surface morphology compared to P3HT thin film. This result indicates that the GS are well embedded in the P3HT matrix. This finding offers a good agreement with the PL quenching phenomenon as we have discussed before since the interfacial area in the P3HT:GS film is increased and thereby facilitates charge separation to form free hole and electron carriers from P3HT to GS within the active layer. Consequently, the addition of GS into P3HT also provides a better pathway for electrons and holes to travel across the active layer and results in an improved performance of PSC (Liu et al., 2013). Table 5.2 summarizes the Ra and RMS for both films. It could be seen that P3HT:GS film exhibits rougher surface compared to pristine P3HT.

Table 5.2 The mean surface roughness and root-mean-square roughness of the film obtained from AFM.

Samples	**Mean surface roughness, Ra (± 0.1) nm**	**Root-mean-square roughness, RMS (± 0.1) nm**
Pristine P3HT	2.5	3.8
P3HT:GS	3.4	4.3

As surface morphology of the PSC is important in order to understand the importance of adding GS in P3HT blend films, in addition to AFM, FESEM is also carried out. FESEM image of P3HT:GS blend film is shown in Figure 5.6. From the FESEM analysis, the presence of GS blended with the P3HT thin film depicted by the presence of GS flakes on the smooth and featureless P3HT film. This result indicates that the GS were well embedded in the P3HT matrix. This finding is consistent with the PL quenching phenomenon since the interface area in the P3HT:GS film increased.

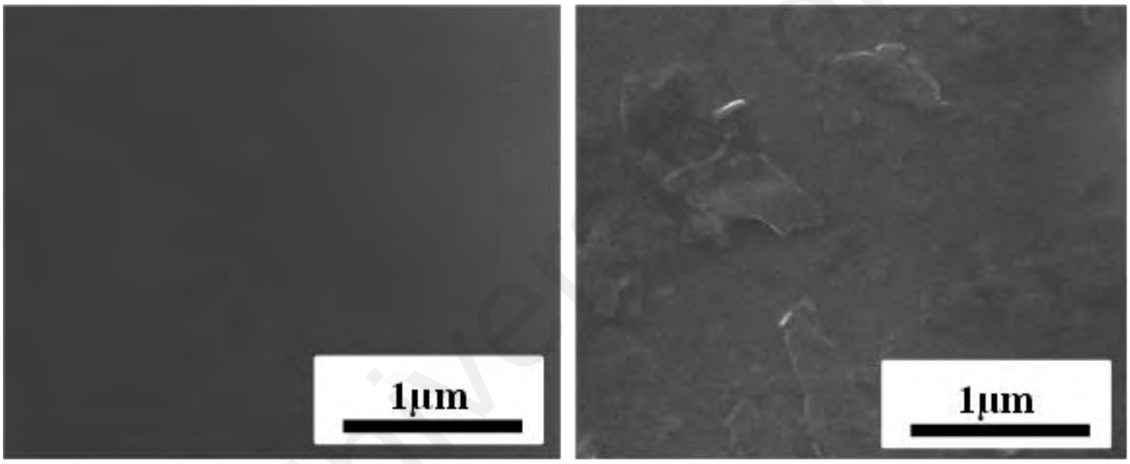

(a) (b)

Figure 5.6: FESEM image of P3HT:GS thin films.

5.3.3 Electrical Characterization

After the fabrication process, the device is subjected to electrical characterization to observe the performance of the device.

5.3.3.1 Current Density-Voltage (J-V) Characteristics

To explore the electrical conduction mechanisms of the devices, the current is shown as a function of the applied bias on a double logarithmic plot. In Figure 5.7, the semilog plot reveals that the current follows a power law in the form of $I \sim V^m$, and three different regimes can be identified. In the first lower voltage regime ($V < 0.7$ V), the currents $I \propto V^m$ where the values of m are 4.4 x 10^{-5} and 1.2 x 10^{-4} for P3HT and P3HT:GS devices, respectively. The values of m in both cases are smaller than unity, which can be attributed to the formation of an aluminium oxide layer between the Al/P3HT:GS and Al/P3HT interfaces. When the applied voltage is increased (0.7 V $< V <$ 1.2 V), the I–V behaviour became bulk controlled, which can be treated as a space-charge-limited current (SCLC) with a single discrete shallow trap of $I \propto V^m$ where the values of m are 0.28 and 0.20 for P3HT and P3HT:GS devices respectively. Further increasing the applied voltage ($V >$ 1.2 V) can be explained by the trap-filling limited current with m = 7.8 and 5.0 for P3HT and P3HT:GS devices, respectively. For Figure 5.8, in the first lower voltage regime (region I), the currents $I \propto V^m$ where the values of m are 0.30 and 0.08 for P3HT and P3HT:GS devices, respectively. Meanwhile, the m value which is obtained from region II is found to be approximately 3.3 and 2.5 for P3HT and P3HT:GS respectively.In region III, the slope of logarithmic J-V curves is approximately 9.3 and 8.0 for P3HT and P3HT:GS respectively which can be explained by the trap-filling limited current as well.

In PSC, higher applied voltages for current measurement are not able to perform due to the thin layers of the organic films which device breakdown usually occurred at approximately 5 V. Besides, other low-molecular-weight organic materials perceived a power-law dependence of the current on the applied voltage as well (Brütting et al., 2001).

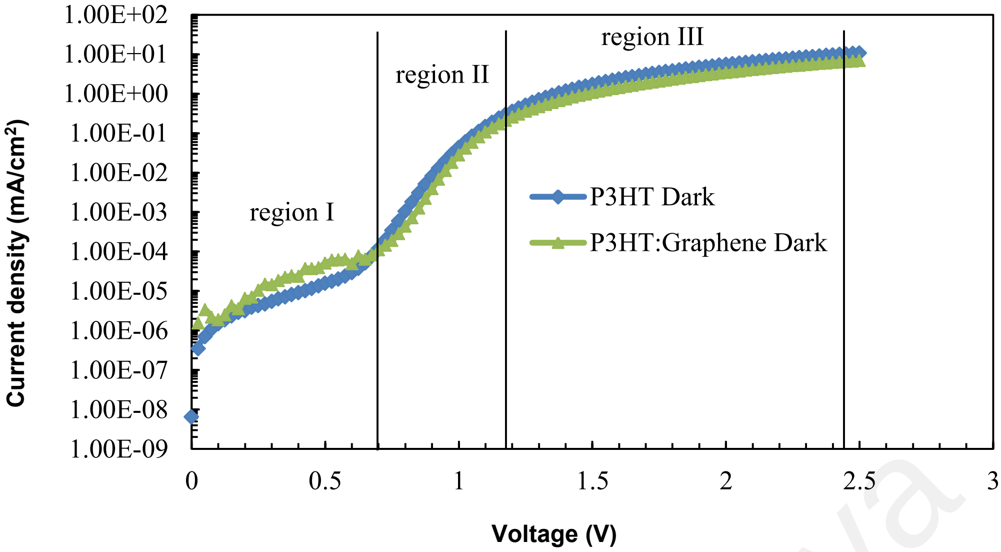

Figure 5.7: Semi-log plot of current density – voltage characteristic of P3HT and P3HT:GS devices under dark.

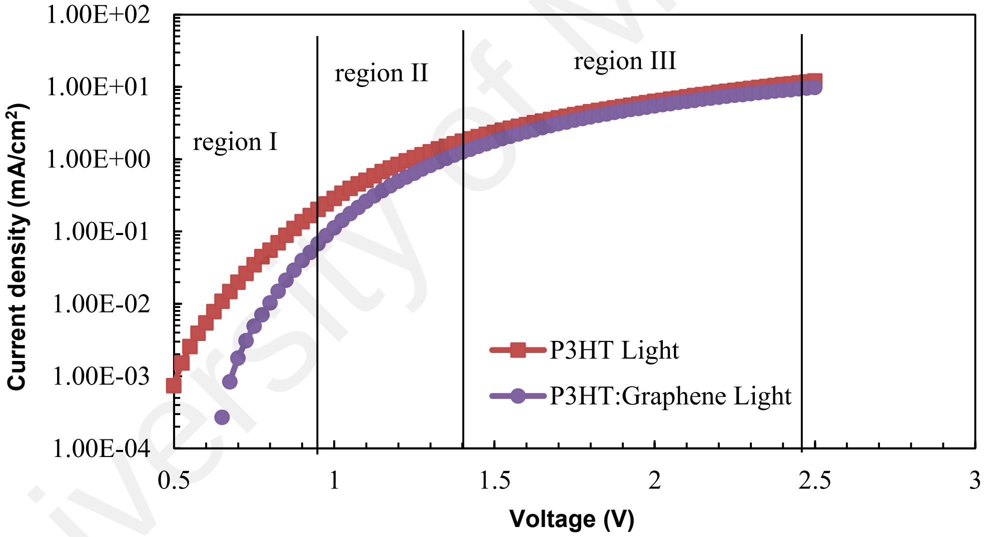

Figure 5.8: Semi-log plot of current density – voltage characteristic of P3HT and P3HT:GS devices under illumination.

5.3.3.2 Solar Cell Power Efficiency

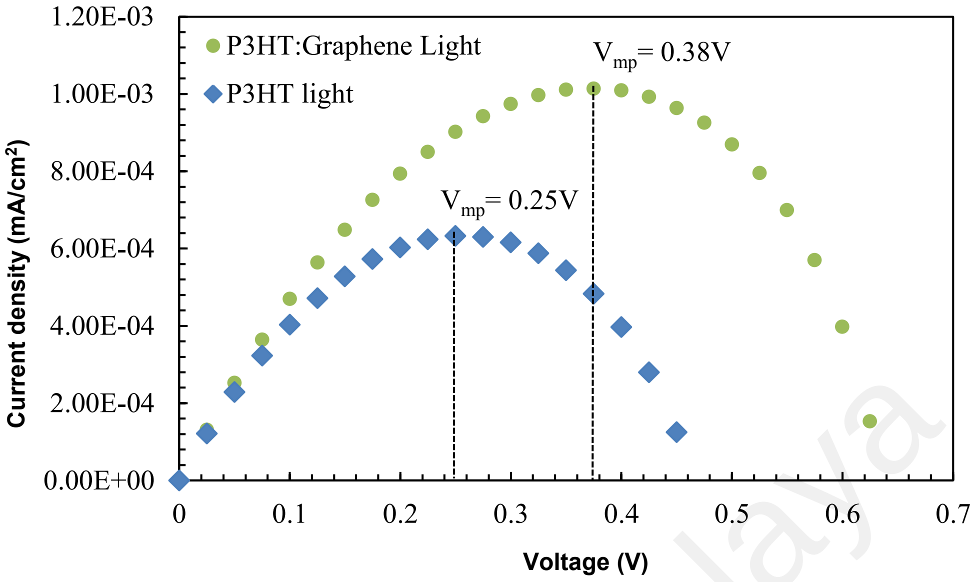

Figure 5.9: Solar cell efficiency curve for pristine P3HT and P3HT:GS device.

For more elucidation of the effect of GS as active layer in solar cell, the Power density–Voltage (*P*–*V*) characteristics are plotted, as shown in Figure 5.9, and estimated V_{oc}/V_{mp} ratio is tabulated in Table 5.5. V_{mp} is the operating voltage of the solar cell devices at a maximum power point (MPP) that is capable to be delivered from the cells. FF is calculated by dividing this power value over the product of open circuit voltage and short circuit current devices (*Voc* × *Jsc*). One can notice that the value of V_{mp} increased with increasing the *V* where V_{mp} of P3HT:GS is higher than pristine P3HT device. The ratio of V_{oc} *to* V_{mp} for both devices are also constant which implies that both devices are still following the rule of PV characteristics curve.

5.3.3.3 Photovoltaic (PV) Characteristics

Figure 5.12 shows the current-voltage (*J-V*) characteristics of the PV devices under illumination based on pristine P3HT and P3HT:GS as well as in the dark. Both *J-V* curves P3HT and P3HT:GS devices exhibit the normal diode-like behaviors in the dark. For the device under light illumination, open-circuit voltage (V_{oc}) is 0.47 V, short-circuit current density (J_{sc}) is 5.1 µA/cm^2 and Fill-factor (*FF*) is 0.26 for pristine P3HT as the active layer. By introducing a small amount of GS into P3HT active layer, V_{oc} of the heterojunction device is increased to 0.65V, J_{sc} is raised to 5.4 µA/cm^2 and *FF* enhanced to 0.29. The photovoltaic characteristics of both devices, open-circuit voltage (V_{oc}), short-current density (J_{sc}), *FF* and power conversion efficiency (η) are tabulated in Table 5.3. For overall performance, power conversion efficiency has been increased from 6.32 x 10^{-4} % (pristine P3HT) to 1.01 x 10^{-3} % (P3HT:GS). Apparently, the addition of GS can raise the device efficiency, indicating that there is a charge transfer from P3HT donor to the GS as acceptor and the PL results support this charge transfer process Tang et al. (1986). proposed that the observed synergistic effect of bringing two different semiconductors in contact is caused by the field at the heterojunction interface, so this local field aids in dissociation of excitons to diffuse to the interface.

Table 5.3: Photovoltaic performance of the investigated PV devices.

Graphene content (%)	**V_{oc} (V)**	**V_{mp} (V)**	**V_{oc}/ V_{mp}**	**J_{sc} (µA/cm^2)**	***FF***	**η (%)**
0%	0.47	0.25	1.88	5.1	0.26	6.32 x 10^{-4}
2.5%	0.65	0.38	1.71	5.4	0.29	1.01 x 10^{-3}

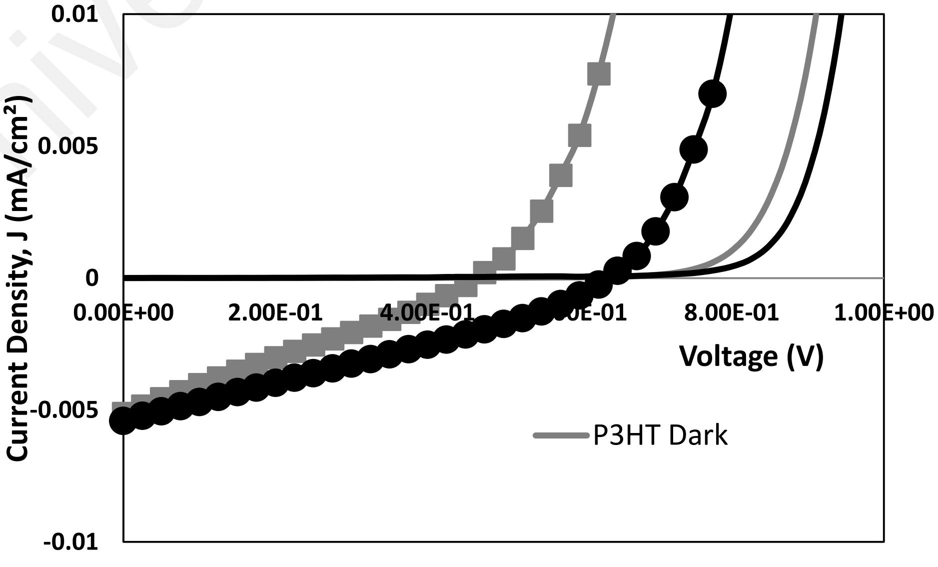

Figure 5.10: The comparison of the *J-V* characteristics of the solar cell devices without and with graphene (GS) under dark and illumination.

5.4 Summary

According to morphological characterizations using AFM and FESEM analysis, the P3HT has shown a relatively smooth surface with a small surface roughness value. Upon the addition of GS, phase separation takes place between the P3HT donor and GS acceptor as can be seen by the increment in surface roughness and morphological features. In this research, the phase separation which take places when doping 2.5% GS into P3HT is one of the crucial factor in order to increase PSC efficiency.

Nevertheless, overall performance of the investigated solar cells in this research work requires further improvement (very low efficiency approximately 3×10^{-3}) in future work, such as through the introduction of an electron acceptor material to form a bulk heterojunction device. The performance of GS based solar cell could be optimized by controlling the sheet resistance and the doping of GS. This bulk heterojunction layer can also be fabricated via a solution-processed spin-coating method such as the kind used in this study. The heterojunction structure can reinforce the dissociation of the exciton, thus generating more efficient charge transfer.

CHAPTER 6: CONCLUSIONS AND FUTURE WORKS

6.1 Conclusion

PSC have many advantages to explore in order to be commercialized in the future. The idea of replacing the acceptor material of PSC with graphene is really worthy in terms of low cost material production compared to high cost of fullerenes. The purpose of this study is to self-synthesize graphene and characterize the P3HT:graphene blend films. Then, this P3HT:graphene blend will be applied in fabricated PSC as an active layer to investigate its ability to enhance the efficiency of the PSC. There are two ways of producing self-synthesized graphene in this study which are via the exfoliation process of graphite flakes into GS and the oxidation process using Hummer's Method. We have successfully obtained GS based on a simple method of exfoliation process and then used the GS as an acceptor in P3HT PSC. The surface morphology as well as optical properties of the P3HT:GS film have been investigated and correlated with device performances. We found that the device performance has been increased with a fill factor of 0.29 by adding a small amount of GS into the active layer. However, the efficiency value is still very low compared to several other hybrid solar cells and needs to be further studied.

6.2 Suggestions for future works

In this study, a facile method in producing graphene via sonication process is successfully achieved. However the difficulties faced are to control the amount and layers of graphene produced. Hence, future works can be done to control the percentage of graphene in solution since the percentage is largely depending on sonication process.

Furthermore, as well known GO is not a conducting material. Therefore two reduction techniques that are hydrothermal and heating techniques can be done to reduce GO, thus forming the reduced graphene oxide (rGO). Usually, rGO produced using both reduction methods tends to form a precipitated agglomerate and did not blend well with any organic solvents due to the π-π stacking interactions. Therefore, functionalization of graphene can be performed via isocyanate treatment in order to chemically introduce new functional groups onto the surface of graphene. The isocyanate treatment can be conducted by two ways which are under nitrogen and solvothermal methods. The final product from both functionalization techniques can be used as an acceptor in future study.

REFERENCES

Adams, W. G., & Day, R. E. (1877). The Action of Light on Selenium. *Philosophical Transactions of the Royal Society of London, 167*, 313–349.

Anjali Y., Aditi U., Saral Kumar G., Ajay Singh V., Chandra Mohan S. N., (2019). Poly-(3-hexylthiophene)/graphene composite based organic photodetectors: The influence of graphene insertion. *Thin Solid Films, 675*, 128-135,

Ahmad, R. (2003). n-Butane and n-Pentane isomerization over sulfated zirconia catalysts investigated by in situ UV-vis-near-IR diffuse reflectance spectroscopy. (Doctral dissertation). Retrieved from https://www.researchgate.net/

Becquerel, A. E. (1839). Recherches sur les effets de la radiation chimique de la lumiere solaire au moyen des courants electriques. *Comptes Rendus de L' Academie Des Sciences, 9*, 145–149.

Bera, M., Chandravati, Gupta, P., & Maji, P. K. (2018). Facile one-pot synthesis of graphene oxide by sonication assisted mechanochemical approach and its surface chemistry. *Journal of Nanoscience and Nanotechnology*, *18*(2), 902-912.

Bharathan, J. M., & Yang, Y. (1998). Polymer/metal interfaces and the performance of polymer light-emitting diodes. *Journal of Applied Physics, 84*(6), 3207–3211.

Bkakri, R., Chehata, N., Ltaief, A., Kusmartseva, O. E., Kusmartsev, F. V., Song, M., & Bouazizi, A. (2015). Effects of the graphene content on the conversion efficiency of P3HT:Graphene based organic solar cells. *Journal of Physics and Chemistry of Solids*, *85*, 206–211.

Boehm, H. P., Clauss, A., Fischer, G. O., & Hofmann, U. (1962). Das adsorptionsverhalten sehr dünner kohlenstoff-folien. *Zeitschrift Für Anorganische Und Allgemeine Chemie, 316*(3-4), 119–127.

Boukhvalov, D. W., & Katsnelson, M. I. (2008). Modeling of graphite oxide. *Journal of the American Chemical Society, 130*(32), 10697–10701.

Brabec, C. J., Sariciftci, N. S., & Hummelen, J. C. (2001). Plastic solar cells. *Advanced Functional Materials, 11*(1), 15–26.

Brabec, C. J., Winder, C., Sariciftci, N. S., Hummelen, J. C., Dhanabalan, A., Van Hal, P. A., & Janssen, R. A. J. (2002). A low-bandgap semiconducting polymer for photovoltaic devices and infrared emitting diodes. *Advanced Functional Materials, 12*(10), 709–712.

Brebels, J., Kesters, J., Defour, M., Pirotte, G., Van Mele, B., Manca, J., Maes, W. (2018). A PCPDTTPD-based narrow bandgap conjugated polyelectrolyte for organic solar cells. *Polymer*, *137*, 303–311.

Brodie, B. C. (1859). On the Atomic Weight of Graphite. *Philosophical Transactions of the Royal Society of London, 149*, 249–259.

Brütting, W., Berleb, S., & Mückl, A. G. (2001). Space-charge limited conduction with a field and temperature dependent mobility in Alq light-emitting devices. *Synthetic Metals, 122*(1), 99-104.

Bube, R. H. (1960). *Photoconductivity of solids*. (R. H. Bube, Ed.). Wiley. Retrieved on 2015 from https://books.google.com.my/

Buchsteiner, A., Lerf, A., & Pieper, J. (2006). Water dynamics in graphite oxide investigated with neutron scattering. *Journal of Physical Chemistry B, 110*(45), 22328–22338.

Burroughes, J. H., Bradley, D. D. C., Brown, A. R., Marks, R. N., Mackay, K., Friend, R. H., Holmes, A. B. (1990). Light-emitting diodes based on conjugated polymers. *Nature, 347*(6293), 539–541.

Cai, W., Piner, R. D., Stadermann, F. J., Park, S., Shaibat, M. A., Ishii, Y., Ruoff, R. S. (2008). Synthesis and solid-state NMR structural characterization of 13c-labeled graphite oxide. *Science, 321*(5897), 1815–1817.

Carsten, B., Szarko, J. M., Son, H. J., Wang, W., Lu, L., He, F. Yu, L. (2011). Examining the effect of the dipole moment on charge separation in donor-acceptor polymers for organic photovoltaic applications. *Journal of the American Chemical Society, 133*(50), 20468–20475.

Chen, H., Müller, M. B., Gilmore, K. J., Wallace, G. G., & Li, D. (2008). Mechanically strong, electrically conductive, and biocompatible graphene paper. *Advanced Materials, 20*(18), 3557–3561.

Chen, L.-M., Hong, Z., Li, G., & Yang, Y. (2009). Recent progress in polymer solar cells: manipulation of polymer:fullerene morphology and the formation of efficient inverted polymer solar cells. *Advanced Materials, 21*(14–15), 1434–1449.

Chiang, C. K., Fincher, C. R., Park, Y. W., Heeger, A. J., Shirakawa, H., Louis, E. J., MacDiarmid, A. G. (1977). Electrical conductivity in doped polyacetylene. *Physical Review Letters, 39*(17), 1098–1101.

Cook, S., Katoh, R., & Furube, A. (2009). Ultrafast studies of charge generation in PCBM:P3HT blend films following excitation of the fullerene PCBM. *The Journal of Physical Chemistry C, 113*(6), 2547-2552.

Dai, L. (1999). Conjugated and fullerene-containing polymers for electronic and photonic applications: advanced syntheses and microlithographic fabrications. *Journal of Macromolecular Science, Part C: Polymer Reviews, 39*(2), 273–387.

Deibel, C., & Dyakonov, V. (2010). Polymer-fullerene bulk heterojunction solar cells. *Reports on Progress in Physics, 73*(9), 96401.

Dikin, D. A., Stankovich, S., Zimney, E. J., Piner, R. D., Dommett, G. H. B., Evmenenko, G., Ruoff, R. S. (2007). Preparation and characterization of graphene oxide paper. *Nature, 448*(7152), 457–460.

Dong, P., Zhu, Y., Zhang, J., Peng, C., Yan, Z., Li, L., Lou, J. (2014). Graphene on metal grids as the transparent conductive material for dye sensitized solar cell. *The Journal of Physical Chemistry C, 118*(45), 25863–25868.

Duan, R., Cui, Y., Zhao, Y., Li, C., Chen, L., Hou, J., Müllen, K. (2016). The importance of end groups for solution-processed small-molecule bulk-heterojunction photovoltaic cells. *ChemSusChem, 9*(9), 973–980.

Eda, G., Fanchini, G., & Chhowalla, M. (2008). Large-area ultrathin films of reduced graphene oxide as a transparent and flexible electronic material. *Nature Nanotechnology, 3*(5), 270–274.

Eletskii, A. V, Zitserman, V. Y., & Kobzev, G. A. (2015). Graphene for solar energy. *Nanotechnologies in Russia, 10*(3), 181–191.

Elias, D. C., Nair, R. R., Mohiuddin, T. M. G., Morozov, S. V., Blake, P., Halsall, M. P., Novoselov, K. S. (2009). Control of graphene's properties by reversible hydrogenation: evidence for graphane. *Science, 323*(5914), 610-613.

Fei Z., Xiao-Yu Y., Peng-Qing B., Meng-Si N., Cheng-Kun L., Lin F., Wei Q., Yu-Zhu W., Xiao-Tao H., Kenneth P. G., (2017). Poly(3-hexylthiophene) coated graphene oxide for improved performance of bulk heterojunction polymer solar cells. *Organic Electronics, 44*, 149-158,

Ferrari, A. C., Meyer, J., Scardaci, V., Casiraghi, C., Lazzeri, M., Mauri, F., Roth, S. (2006). Raman spectrum of graphene and graphene layers. *Physical Review Letters, 97*(18), 187401.

Forrest, S. R. (2004). The path to ubiquitous and low-cost organic electronic appliances on plastic. *Nature, 428*(6986), 911–918.

Friend, R. H., Denton, G. J., Halls, J. J. M., Harrison, N. T., Holmes, A. B., Köhler, A., Towns, K. (1997). Electronic processes of conjugated polymers in semiconductor device structures. *Synthetic Metals, 84*(1–3), 463–470.

Fujii, T., Nishikiori, H., & Tamura, T. (1995). Absorption spectra of rhodamine B dimers in dip-coated thin films prepared by the sol-gel method. *Chemical Physics Letters, 233*(4), 424–429.

Gao, P., Ding, K., Wang, Y., Ruan, K., Diao, S., Zhang, Q., … Jie, J. (2014). Crystalline si/graphene quantum dots heterojunction solar cells. *The Journal of Physical Chemistry C, 118*(10), 5164–5171.

Geim, A. K., & Novoselov, K. S. (2007). The rise of graphene. *Nature Materials, 6*, 183-191.

Goetzberger, A., Hebling, C., & Schock, H.-W. (2003). Photovoltaic materials, history, status and outlook. *Materials Science and Engineering: R: Reports, 40*(1), 1–46.

Greenham, N. C., Moratti, S. C., Bradley, D. D. C., Friend, R. H., & Holmes, A. B. (1993). Efficient light-emitting diodes based on polymers with high electron affinities. *Nature, 365*(6447), 628–630.

Günes, S., Neugebauer, H., & Sariciftci, N. S. (2007). Conjugated polymer-based organic solar cells. *Chemical Reviews, 107*(4), 1324–1338.

Harrison, W. A. (1979). Theory of polar semiconductor surfaces. *Journal of Vacuum*

Science and Technology, 16(5), 1492–1496.

He, H., Klinowski, J., Forster, M., & Lerf, A. (1998). A new structural model for graphite oxide. *Chemical Physics Letters, 287*(1–2), 53–56.

He, H., Riedl, T., Lerf, A., & Klinowski, J. (1996). Solid-State NMR Studies of the Structure of Graphite Oxide. *The Journal of Physical Chemistry, 100*(51), 19954–19958.

Heeger, A. J. (2001). Semiconducting and metallic polymers: the fourth generation of polymeric materials. *The Journal of Physical Chemistry B, 105*(36), 8475–8491.

Hummers, W. S., & Offeman, R. E. (1958). Preparation of Graphitic Oxide. *Journal of the American Chemical Society, 80*(6), 1339.

Jeon, Y.-J., Yun, J.-M., Kim, D.-Y., Na, S.-I., & Kim, S.-S. (2014). Moderately reduced graphene oxide as hole transport layer in polymer solar cells via thermal assisted spray process. *Applied Surface Science, 296*, 140–146.

Ju, H.-M., Huh, S. H., Choi, S.-H., & Lee, H.-L. (2010). Structures of thermally and chemically reduced graphene. *Materials Letters, 64*(3), 357-360.

Jung, I., Pelton, M., Piner, R., Dikin, D. A., Stankovich, S., Watcharotone, S., Ruoff, R. S. (2007). Simple approach for high-contrast optical imaging and characterization of graphene-based sheets. *Nano Letters, 7*(12), 3569–3575.

Kearns, D., & Calvin, M. (1958). Photovoltaic Effect and Photoconductivity in Laminated Organic Systems. *The Journal of Chemical Physics, 29*(4), 950–951.

Kietzke, T. (2007). Recent Advances in Organic Solar Cells. *Advances in OptoElectronics, 2007*, Article ID 40285, 1-15.

Kim, J. S., Granström, M., Friend, R. H., Johansson, N., Salaneck, W. R., Daik, R., Cacialli, F. (1998). Indium–tin oxide treatments for single- and double-layer polymeric light-emitting diodes: The relation between the anode physical, chemical, and morphological properties and the device performance. *Journal of Applied Physics, 84*(12), 6859–6870.

Kim, K., Bae, S.-H., Toh, C. T., Kim, H., Cho, J. H., Whang, D., Ahn, J.-H. (2014). Ultrathin organic solar cells with graphene doped by ferroelectric polarization. *ACS Applied Materials & Interfaces, 6*(5), 3299–3304.

Kim, S. G., Park O. K., Lee J., & Ku B. C. (2013). Layer-by-layer assembled graphene oxide films and barrier properties of thermally reduced graphene oxide membranes. *Carbon letters. 14*(4). 247-250.

Kabongo, G. L., Mbule, P. S., Mhlongo, G. H., Mothudi, B. M., Hillie, K. T., & Dhlamini, M. S. (2016). Photoluminescence quenching and enhanced optical conductivity of P3HT-Derived Ho^{3+}-Doped ZnO nanostructures. *Nanoscale Research Letters, 11*(1), 418. 1-11.

Lai, Q., Zhu, S., Luo, X., Zou, M., & Huang, S. (2012). Ultraviolet-visible spectroscopy of graphene oxides. *AIP Advances, 2*(3), 032146. 1-5.

Landau, L. D. (1937). On the theory of phase transitions. *The Journal of Experimental and Theoretical Physics, 7*, 19–32.

Landau, L., & Lifshitz, E. (1980). *Statistical Physics: Part 1 – Third Edition, Vol. 5. Course of Theoretical Physics.* Moscow, Russia: Pergamon Press.

Lerf, A., Buchsteiner, A., Pieper, J., Schöttl, S., Dekany, I., Szabo, T., & Boehm, H. P. (2006). Hydration behavior and dynamics of water molecules in graphite oxide. *Journal of Physics and Chemistry of Solids, 67*(5–6), 1106–1110.

Lerf, A., He, H., Forster, M., & Klinowski, J. (1998). Structure of graphite oxide revisited. *The Journal of Physical Chemistry B, 102*(23), 4477–4482.

Li, D., Müller, M. B., Gilje, S., Kaner, R. B., & Wallace, G. G. (2008). Processable aqueous dispersions of graphene nanosheets. *Nature Nanotechnology, 3*(2), 101–105.

Li, G., Budiawan, W., Wang, P.-C., & Wei Chu, C. (2018). Conjugated polymer-based solar cells. *Encyclopedia of Modern Optics*, *5*, 256–269.

Li, G., Shrotriya, V., Huang, J., Yao, Y., Moriarty, T., Emery, K., & Yang, Y. (2005). High-efficiency solution processable polymer photovoltaic cells by self-organization of polymer blends. *Nature Materials, 4*(11), 864-868.

Li, G., Zhu, R., & Yang, Y. (2012). Polymer solar cells. *Nature Photonics, 6*, 153-161.

Li, Y., & Qian, R. (1993). Stability of conducting polymers from the electrochemical point of view. *Synthetic Metals, 53*(2), 149–154.

Liang, Y., Xu, Z., Xia, J., Tsai, S.-T., Wu, Y., Li, G., Yu, L. (2010). For the bright future - bulk heterojunction polymer solar cells with power conversion efficiency of 7.4%. *Advanced Materials, 22*(20), 135–138.

Liu, Y., Chen, C.-C., Hong, Z., Gao, J., Yang, Y., Zhou, H., Yang, Y. (2013). Solution-processed small-molecule solar cells: breaking the 10% power conversion efficiency. *Scientific Reports, 3*, 3356. 1-8.

Liu, Y., Zhao, J., Li, Z., Mu, C., Ma, W., Hu, H., Yan, H. (2014). Aggregation and morphology control enables multiple cases of high-efficiency polymer solar cells. *Nature Communications, 5*, 5293. 1-8.

Liu, Z., He, D., Wang, Y., Wu, H., & Wang, J. (2010). Solution-processable functionalized graphene in donor/acceptor-type organic photovoltaic cells. *Solar Energy Materials and Solar Cells, 94*(7), 1196-1200.

Lomeda, J. R., Doyle, C. D., Kosynkin, D. V., Hwang, W. F., & Tour, J. M. (2008). Diazonium functionalization of surfactant-wrapped chemically converted graphene sheets. *Journal of the American Chemical Society, 130*(48), 16201–16206.

Ma, C., Yang, K., Wang, L., & Wang, X. (2017). Facile synthesis of reduced graphene oxide/fe3o4 nanocomposite film. *Journal of Applied Biomaterials & Functional Materials, 15*(Suppl 1), S1-S6.

Ma, W., Yang, C., Gong, X., Lee, K., & Heeger, A. J. (2005). Thermally stable, efficient polymer solar cells with nanoscale control of the interpenetrating network morphology. *Advanced Functional Materials, 15*(10), 1617–1622.

MacDiarmid, A. G. (2001). "Synthetic metals": A novel role for organic polymers. *Angewandte Chemie International Edition, 40*(14), 2581–2590.

Malaysian Energy Commission. (2015). *National Energy Balance*. Putrajaya: Malaysia.

McAllister, M. J., Li, J. L., Adamson, D. H., Schniepp, H. C., Abdala, A. A., Liu, J., Aksay, I. A. (2007). Single sheet functionalized graphene by oxidation and thermal expansion of graphite. *Chemistry of Materials, 19*(18), 4396–4404.

McClure, J. W. (1956). Diamagnetism of graphite. *Physical Review, 104*(3), 666–671.

Menke, S. M., Ran, N. A., Bazan, G. C., & Friend, R. H. (2018). Understanding energy loss in organic solar cells: Toward a new efficiency regime. *Joule, 2*(1), 25–35.

Mermin, N. D. (1968). Crystalline order in two dimensions. *Physical Review, 176*(1), 250–254.

Meyer, J. C., Geim, A. K., Katsnelson, M. I., Novoselov, K. S., Booth, T. J., & Roth, S. (2007). The structure of suspended graphene sheets. *Nature, 446*, 60–63.

Michaelson, H. B. (1977). The work function of the elements and its periodicity. *Journal of Applied Physics, 48*(11), 4729.

Miles, R. W., Zoppi, G., & Forbes, I. (2007). Inorganic photovoltaic cells. *Materials Today, 10*(11), 20–27.

Morozov, S. V., Novoselov, K. S., Katsnelson, M. I., Schedin, F., Elias, D. C., Jaszczak, J. A., & Geim, A. K. (2008). Giant intrinsic carrier mobilities in graphene and its bilayer. *Physical Review Letters, 100*(1), 16602.

Muhammad, F. F., Abdul Hapip, A. I., & Sulaiman, K. (2010). Study of optoelectronic energy bands and molecular energy levels of tris (8-hydroxyquinolinate) gallium and aluminum organometallic materials from their spectroscopic and electrochemical analysis. *Journal of Organometallic Chemistry, 695*(23), 2526–2531.

Muszynski, R., Seger, B., & Kamat, P. V. (2008). Decorating graphene sheets with gold nanoparticles. *Journal of Physical Chemistry C, 112*(14), 5263–5266.

Muthu, R. N., Rajashabala, S., & Kannan, R. (2016). Facile synthesis and characterization of a reduced graphene oxide/halloysite nanotubes/hexagonal boron nitride (RGO/HNT/h-BN) hybrid nanocomposite and its potential application in hydrogen storage. *RSC Advances, 6*(82), 79072–79084.

Naebe, M., Wang, J., Amini, A., Khayyam, H., Hameed, N., Li, L. H., Fox, B. (2014). Mechanical property and structure of covalent functionalised graphene/epoxy nanocomposites. *Scientific Reports, 4*, 4375.

Niyogi, S., Bekyarova, E., Itkis, M. E., McWilliams, J. L., Hamon, M. A., & Haddon, R. C. (2006). Solution properties of graphite and graphene. *Journal of the American*

Chemical Society, 128(24), 7720–7721.

Novoselov, K. S., Geim, A. K., Morozov, S. V., Jiang, D., Zhang, Y., Dubonos, S. V., Firsov, A. A. (2004). Electric field effect in atomically thin carbon films. *Science, 306*(5696), 666–669.

Novoselov, K. S., Jiang, D., Schedin, F., Booth, T. J., Khotkevich, V. V., Morozov, S. V., & Geim, A. K. (2005). Two-dimensional atomic crystals. *Proceedings of the National Academy of Sciences, 102*(30), 10451–10453.

NREL, & National Renewable Energy Laboratory. (2019). Research cell efficiency records. In national center for photovoltaics (NCPV) at NREL (pp. 1–1). http://doi.org/http://www.nrel.gov

O'Regan, B., & Grätzel, M. (1991). A low-cost, high-efficiency solar cell based on dye-sensitized colloidal TiO_2 films. *Nature, 353*, 737–740.

Oganov, A. R., Hemley, R. J., Hazen, R. M., & Jones, A. P. (2013). Structure, bonding, and mineralogy of carbon at extreme conditions. *Reviews in Mineralogy and Geochemistry, 75*(1), 47–77.

Ossonon, B. D., & Bélanger, D. (2017a). Functionalization of graphene sheets by the diazonium chemistry during electrochemical exfoliation of graphite. *Carbon, 111*, 83-93.

Ossonon, B. D., & Bélanger, D. (2017b). Synthesis and characterization of sulfophenyl-functionalized reduced graphene oxide sheets. *RSC Advances, 7*(44), 27224-27234.

P. Aruna, C.M. Joseph, (2017). Annealing effects on the electrical properties of spin coated poly (3-hexylthiophene) (P3HT) thin films, *Materials Science in Semiconductor Processing, 61*, 39-44,

Parades, J. I., Villar-Rodil, S., Martínez-Alonso, A., & Tascón, J. M. D. (2008). Graphene oxide dispersions in organic solvents. *Langmuir, 24*(19), 10560–10564.

Park, S., An, J., Piner, R. D., Jung, I., Yang, D., Velamakanni, A., Ruoff, R. S. (2008). Aqueous suspension and characterization of chemically modified graphene sheets. *Chemistry of Materials, 20*(21), 6592–6594.

Park, S., Lee, K. S., Bozoklu, G., Cai, W., Nguyen, S. B. T., & Ruoff, R. S. (2008). Graphene oxide papers modified by divalent ions - Enhancing mechanical properties via chemical cross-linking. *ACS Nano, 2*(3), 572–578.

Park, Y., Choong, V., Ettedgui, E., Gao, Y., Hsieh, B. R., Wehrmeister, T., & Müllen, K. (1996). Energy level bending and alignment at the interface between Ca and a phenylene vinylene oligomer. *Applied Physics Letters, 69*(8), 1080–1082.

Park, Y., Choong, V., Gao, Y., Hsieh, B. R., & Tang, C. W. (1996). Work function of indium tin oxide transparent conductor measured by photoelectron spectroscopy. *Applied Physics Letters, 68*(19), 2699–2701.

Peierls, R. E. (1935). Quelques proprietes typiques des corpses solides. *Annales De L' Institut H. Poincare, 5*(3), 177–222.

Petit, T., & Puskar, L. (2018). FTIR spectroscopy of nanodiamonds: Methods and interpretation. *Diamond and Related Materials, 89,* 52–66.

Pham, V. H., Cuong, T. V., Hur, S. H., Oh, E., Kim, E. J., Shin, E. W., & Chung, J. S. (2011). Chemical functionalization of graphene sheets by solvothermal reduction of a graphene oxide suspension in N-methyl-2-pyrrolidone. *Journal of Materials Chemistry, 21*(10), 3371-3377.

Pochettino, A. (1906). Sul comportamento foto-elettrico dell'antracene. *Accademia dei Lincei, 15*, 355–368.

Pumera, M., Ambrosi, A., Bonanni, A., Chng, E. L. K., & Poh, H. L. (2010). Graphene for electrochemical sensing and biosensing. *TrAC - Trends in Analytical Chemistry, 29*(9), 954–965.

R. Bkakri, N. Chehata, A. Ltaief, O.E. Kusmartseva, F.V. Kusmartsev, M. Song, A. Bouazizi, (2015). Effects of the graphene content on the conversion efficiency of P3HT:Graphene based organic solar cells, *Journal of Physics and Chemistry of Solids, 85*, 206-211,

Rajagopalan, B., & Chung, J. S. (2014). Reduced chemically modified graphene oxide for supercapacitor electrode. *Nanoscale Research Letters, 9*(1), 535.

Ramírez, A., López N. E., Soboyejo, W., Meas Y. & Vilquin, B. (2015). A Review on the Efficiency of Graphene-Based BHJ Organic Solar Cells. *Journal of Nanomaterials*, *2015*(3). 1-15.

Rand, B. P., Xue, J., Uchida, S., & Forrest, S. R. (2005). Mixed donor-acceptor molecular heterojunctions for photovoltaic applications. I. material properties. *Journal of Applied Physics, 98*(12), 124902.

Reyes-Reyes, M., Kim, K., & Carroll, D. L. (2005). High-efficiency photovoltaic devices based on annealed poly(3-hexylthiophene) and 1-(3-methoxycarbonyl)-propyl-1-phenyl- (6,6) C61 blends. *Applied Physics Letters, 87*(8), 83506.

Sasikala, S. P., Henry, L., Yesilbag Tonga, G., Huang, K., Das, R., Giroire, B., Aymonier, C. (2016). High yield synthesis of aspect ratio controlled graphenic materials from anthracite coal in supercritical fluids. *ACS Nano, 10*(5), 5293–5303.

Schniepp, H. C., Li, J. L., McAllister, M. J., Sai, H., Herrera-Alonson, M., Adamson, D. H., Aksay, I. A. (2006). Functionalized single graphene sheets derived from splitting graphite oxide. *Journal of Physical Chemistry B, 110*(17), 8535–8539.

Scholz, W., & Boehm, H. P. (1969). Untersuchungen am graphitoxid. VI. Betrachtungen zur struktur des graphitoxids. ZAAC *Journal of Inorganic and General Chemistry, 369*(3–6), 327–340.

Shaheen, S. E., Brabec, C. J., Sariciftci, N. S., Padinger, F., Fromherz, T., & Hummelen, J. C. (2001). 2.5% efficient organic plastic solar cells. *Applied Physics Letters, 78*(6), 841–843.

Shirakawa, H. (2001). The discovery of polyacetylene film: the dawning of an era of conducting polymers. *Angewandte Chemie International Edition, 40*(14), 2574–

2580.

Si, Y., & Samulski, E. T. (2008). Synthesis of water soluble graphene. *Nano Letters, 8*(6), 1679–1682.

Slonczewski, J. C., & Weiss, P. R. (1958). Band structure of graphite. *Physical Review, 109*(2), 272–279.

Spanggaard, H., & Krebs, F. C. (2004). A brief history of the development of organic and polymeric photovoltaics. *Solar Energy Materials and Solar Cells, 83*(2–3), 125–146.

Stankovich, S., Dikin, D. A., Dommett, G. H. B., Kohlhaas, K. M., Zimney, E. J., Stach, E. A., Ruoff, R. S. (2006). Graphene-based composite materials. *Nature, 442*(7100), 282–286.

Stankovich, S., Dikin, D. A., Piner, R. D., Kohlhaas, K. A., Kleinhammes, A., Jia, Y., Ruoff, R. S. (2007). Synthesis of graphene-based nanosheets via chemical reduction of exfoliated graphite oxide. *Carbon, 45*(7), 1558–1565.

Stankovich, S., Piner, R. D., Chen, X., Wu, N., Nguyen, S. T., & Ruoff, R. S. (2006). Stable aqueous dispersions of graphitic nanoplatelets via the reduction of exfoliated graphite oxide in the presence of poly(sodium 4-styrenesulfonate). *Journal of Materials. Chemistry, 16*(2), 155–158.

Stankovich, S., Piner, R. D., Nguyen, S. B. T., & Ruoff, R. S. (2006). Synthesis and exfoliation of isocyanate-treated graphene oxide nanoplatelets. *Carbon, 44*(15), 3342–3347.

Staudenmaier, L. (1898). Verfahren zur Darstellung der Graphitsaure. *Berichte Der Deutschen Chemischen Gesellschaft, 31*(2), 1481–1487.

Sze, S. M., & Ng, K. K. (2007). *Physics of Semiconductor Devices - Third edition*, John Wiley & Sons, Inc.

Takahashi, A., Lin, C.-J., Ohshimizu, K., Higashihara, T., Chen, W.-C., & Ueda, M. (2012). Synthesis and characterization of novel polythiophenes with graphene-like structures via intramolecular oxidative coupling. *Polymer Chemistry, 3*(2), 479-485.

Tang, C. W. (1986). Two-layer organic photovoltaic cell. *Applied Physics Letters, 48*(2), 183–185.

Tang, C. W., & Albrecht, A. C. (1975). Photovoltaic effects of metal-chlorophyll-a-metal sandwich cells. *The Journal of Chemical Physics, 62*(6), 2139‑2149.

Tasis, D., Tagmatarchis, N., Bianco, A., & Prato, M. (2006). Chemistry of carbon nanotubes. *Chemical Reviews, 106*(3), 1105–1136.

Thompson, B. C., Kim, Y.-G., & Reynolds, J. R. (2005). Spectral broadening in MEH-PPV:PCBM-based photovoltaic devices via blending with a narrow band gap cyanovinylene−dioxythiophene polymer. *Macromolecules, 38*(13), 5359–5362.

Tim L., Matilde E., Fabiola L., Silvia M., Georgian M., Ovidiu E., Michael S., Artur C., Paolo S., (2018). Graphene exfoliation in the presence of semiconducting polymers for improved film homogeneity and electrical performances, *Carbon, 130*, 495-502,

Tung, V. C., Allen, M. J., Yang, Y., & Kaner, R. B. (2009). High-throughput solution processing of large-scale graphene. *Nature Nanotechnology, 4*(1), 25–29.

Volmer, M. (1913). Die verschiedenen lichtelektrischen erscheinungen am anthracen, ihre beziehungen zueinander, zur fluoreszenz und dianthracenbildung. *Annalen Der Physik, 345*(4), 775–796.

Wallace, P. R. (1947). The band theory of graphite. *Physical Review, 71*(9), 622–634.

Wang, L., Lee, K., Sun, Y.-Y., Lucking, M., Chen, Z., Zhao, J. J., & Zhang, S. B. (2009). Graphene oxide as an ideal substrate for hydrogen storage. *ACS Nano, 3*(10), 2995-3000.

Wang, N., Yang, W., Li, S., Shi, M., Lau, T.-K., Lu, X., Chen, H. (2019). A non-fullerene acceptor enables efficient P3HT-based organic solar cells with small voltage loss and thickness insensitivity. *Chinese Chemical Letters*. (In Press)

Wang, G., Yang, J., Park, J., Gou, X., Wang, B., Liu, H., & Yao, J. (2008). Facile synthesis and characterization of graphene nanosheets. *The Journal of Physical Chemistry C, 112*(22), 8192–8195.

Williams, G., Seger, B., & Kamt, P. V. (2008). TiO_2-graphene nanocomposites. UV-assisted photocatalytic reduction of graphene oxide. *ACS Nano, 2*(7), 1487–1491.

Wöhrle, D., & Meissner, D. (1991). Organic solar cells. *Advanced Materials, 3*(3), 129–138.

Worsley, K. A., Ramesh, P., Mandal, S. K., Niyogi, S., Itkis, M. E., & Haddon, R. C. (2007). Soluble graphene derived from graphite fluoride. *Chemical Physics Letters, 445*(1–3), 51–56.

Xu, B., & Holdcroft, S. (1993). Molecular control of luminescence from poly(3-hexylthiophenes). *Macromolecules, 26*(17), 4457-4460.

Xu, Y., Bai, H., Lu, G., Li, C., & Shi, G. (2008). Flexible graphene films via the filtration of water-soluble noncovalent functionalized graphene sheets. *Journal of the American Chemical Society, 130*(18), 5856–5857.

Xue, J., Rand, B. P., Uchida, S., & Forrest, S. R. (2005). A hybrid planar-mixed molecular heterojunction photovoltaic cell. *Advanced Materials, 17*(1), 66–71.

Yongli C., Guizhong Z., Yating Z., Xiaolong C., Mingxuan C., Yu Y., Haitao D., Jianquan Y., (2018). Solution-processed graphene phototransistor functionalized with P3HT/graphene bulk heterojunction, *Optics Communications, 425*, 161-165,

Zhang, Y. B., Tan, Y. W., Stormer, H. L., & Kim, P. (2005). Experimental observation of the quantum Hall effect and Berry's phase in graphene. *Nature, 438*(7065), 201–204.

Zhao, G. J., He, Y. J., & Li, Y. (2010). 6.5% efficiency of polymer solar cells based on poly(3-hexylthiophene) and indene-C60 bisadduct by device optimization. *Advanced Materials, 22*(39), 4355–4358.

Zhou, H., Yang, L., Stuart, A. C., Price, S. C., Liu, S., & You, W. (2011). Development of fluorinated benzothiadiazole as a structural unit for a polymer solar cell of 7% efficiency. *Angewandte Chemie - International Edition, 50*(13), 2995–2998.

LIST OF PUBLICATIONS AND PAPERS PRESENTED

Publications:

1. **Abd Wahab, F.**, Sulaiman, K., & Huang, N. M. (2013). Synthesis of graphene sheets and characterization of poly(3-hexylthiophene):graphene blends. *Journal of Electronic Materials*, *42*(9), 2739-2742.

2. Sulaiman, K., Ahmad, Z., Fakir, M. S., **Abd Wahab, F.**, Mah Abdullah, S., & Abdul Rahman, Z. (2013). Organic semiconductors: applications in solar photovoltaic and sensor devices. *Materials Science Forum*, *737*, 126-132.

3. Abdul Hapip, A.I., **Abd Wahab, F.**, & Sulaiman, K. (2011). Influence of poly(3-alkylthiophene) (P3ATs) structure on P3AT/Gaq3 films for organic solar cells. *Materials Research Innovations*, *15*(s2), 198-201.

Papers presented:

1. **Abd Wahab, F**., Sulaiman, K., & Huang, N.M. "Investigation on the effects of graphene as an acceptor in polymeric-based solar cells". Paper presented at Nanotechnology Applications in Energy and Environment (NAEE 2012) in Bandung, Indonesia.

2. **Abd Wahab, F.**, Sulaiman, K., & Huang N. M. "Investigation on the effects of graphene as an acceptor in polymeric-based solar cells". Paper presented at 26th Regional Conference of Solid State Science & Technology (RCSSST 2011) in Seremban, Malaysia.